MECHANICAL PROPERTIES

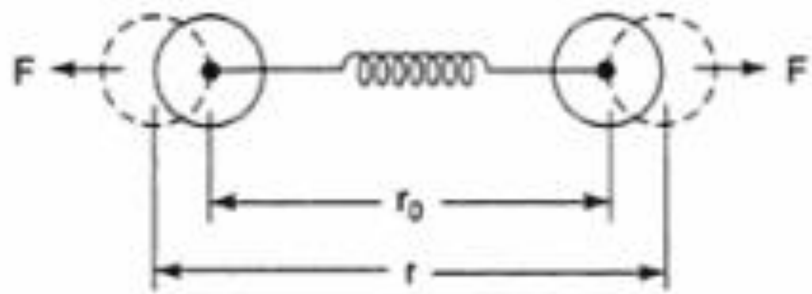

Figure 5.1 Schematic illustration of "bead-and-spring" model of atomic force between atoms. Reprinted, by permission, from M. F. Ashby and D. R. H. Jones, *Engineering Materials 1*, 2nd ed., p. 44. Copyright © 1996 by Michael F. Ashby and David R. H. Jones.

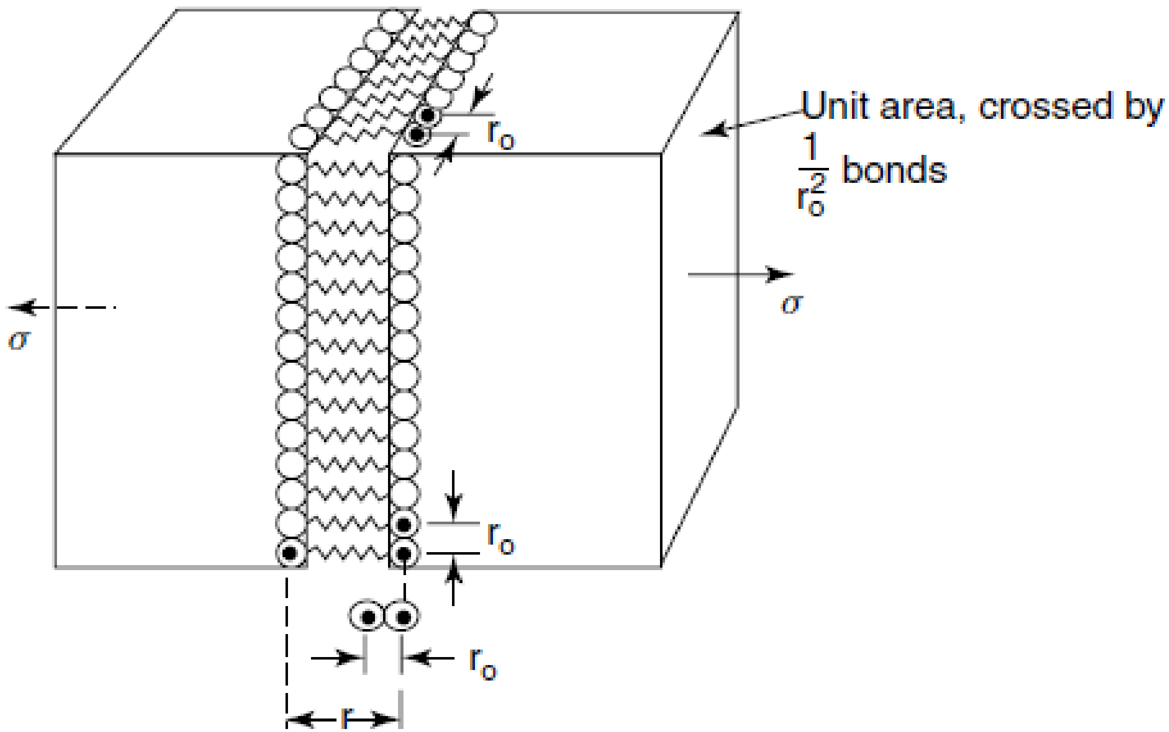

Figure 5.2 Illustration of multiple bead-and-springs in tensile separation of atomic planes. Reprinted, by permission, from M. R. Ashby and D. R. H. Jones, *Engineering Materials 1*, 2nd ed., p. 59, Copyright © 1996 by Michael F. Ashby and David R. H. Jones.

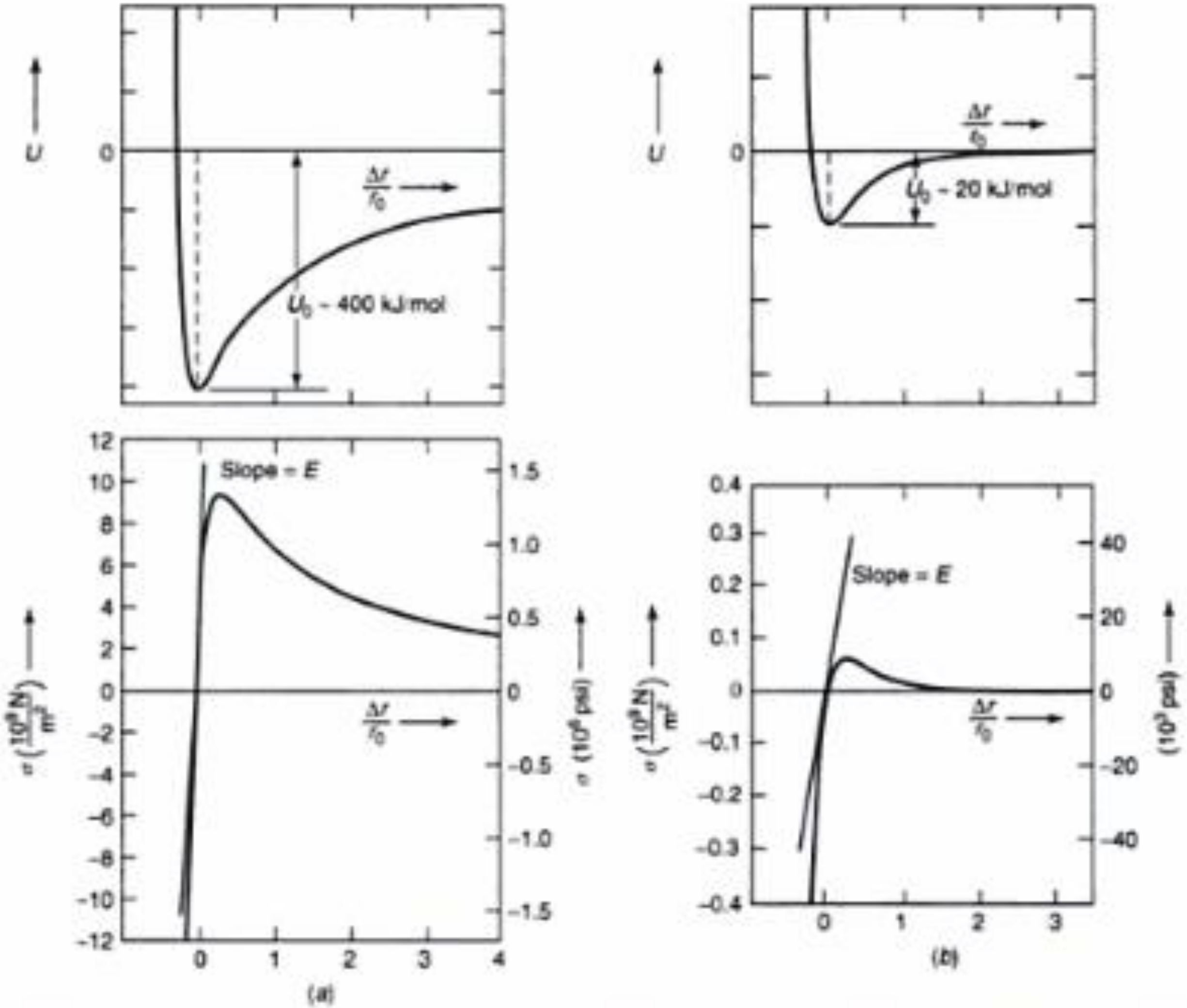

Figure 5.3 Schematic diagrams showing potential energy (*top*) and applied stress (*bottom*) versus linear strain for crystalline solids with (a) strong bonds and (b) weak bonds. From K. M. Ralls, T. H. Courtney, and J. Wulff, *Introduction to Materials Science and Engineering*. Copyright © 1976 by John Wiley & Sons, Inc. This material is used by permission John Wiley & Sons, Inc.

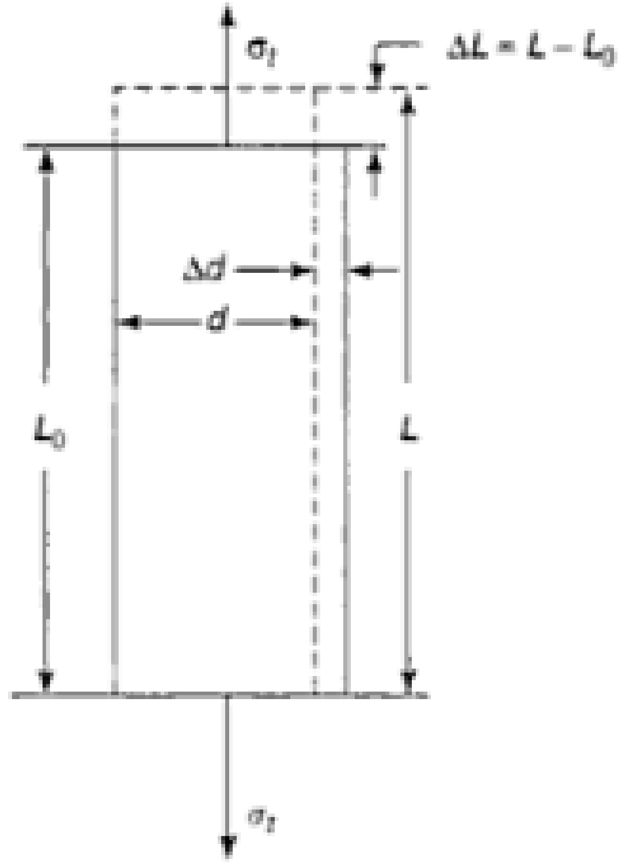

Figure 5.5 Schematic illustration of tensile strain and corresponding lateral strain. From Z. Jastrzebski, *The Nature and Properties of Engineering Materials*, 2nd ed. Copyright © 1976 by John Wiley & Sons, Inc. This material is used by permission of John Wiley & Sons, Inc.

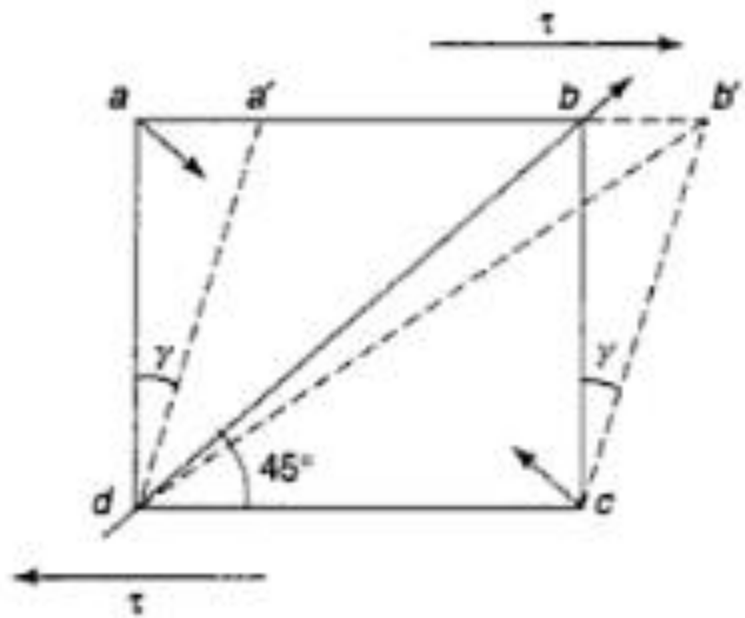

Figure 5.6 Schematic illustration of shear strain and stress. From Z. Jastrzebski, *The Nature and Properties of Engineering Materials*, 2nd ed. Copyright © 1976 by John Wiley & Sons, Inc. This material is used by permission of John Wiley & Sons, Inc.

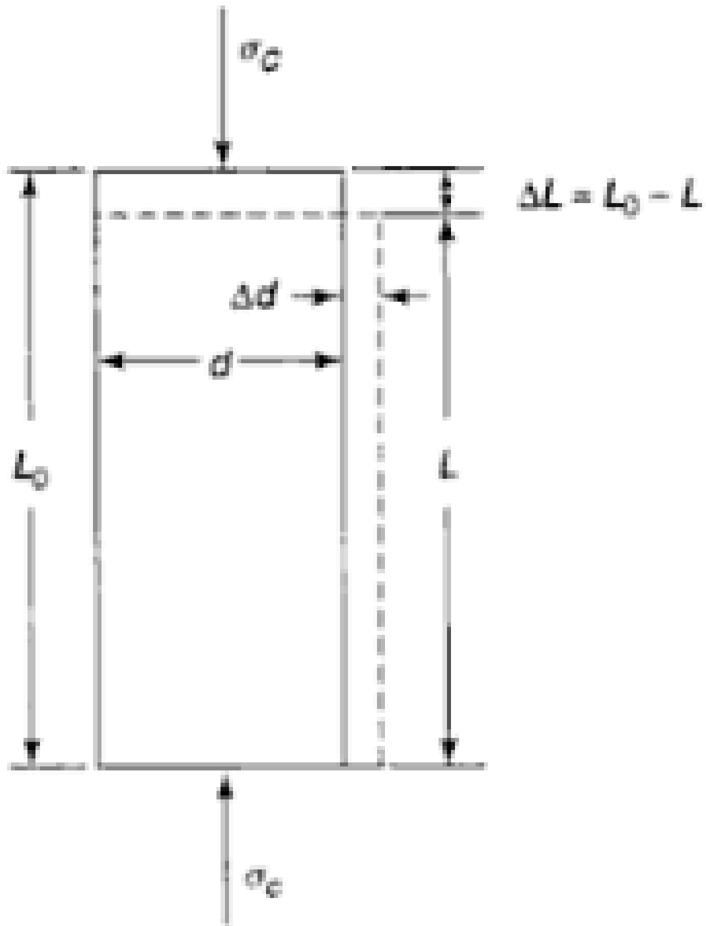

Figure 5.7 Schematic illustration of compressive strain and lateral strain. From Z. Jastrzebski, *The Nature and Properties of Engineering Materials*, 2nd ed. Copyright © 1976 by John Wiley & Sons, Inc. This material is used by permission of John Wiley & Sons, Inc.

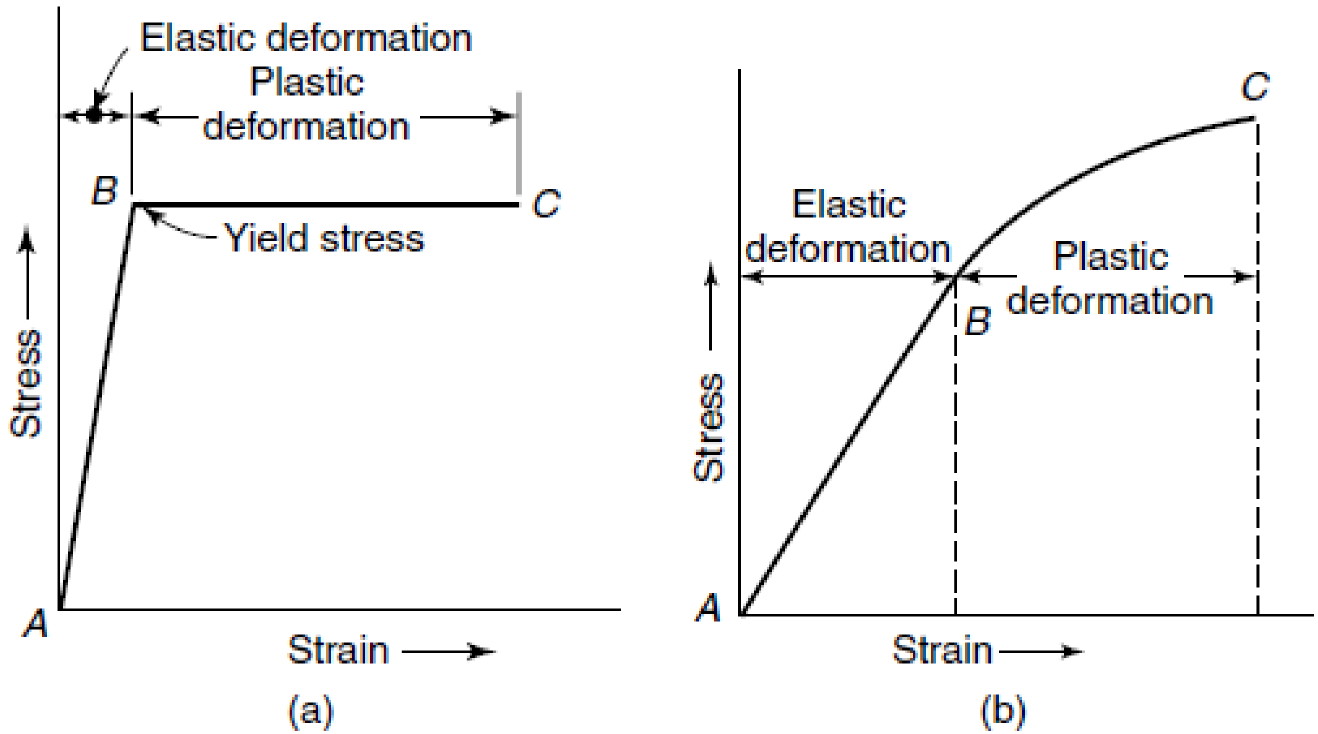

Figure 5.8 Illustration of (a) ideal elastic deformation followed by ideal plastic deformation and (b) typical elastic and plastic deformation in rigid bodies. From Z. Jastrzebski, *The Nature and Properties of Engineering Materials*, 2nd ed., Copyright © 1976 by John Wiley & Sons, Inc. This material is used by permission of John Wiley & Sons, Inc.

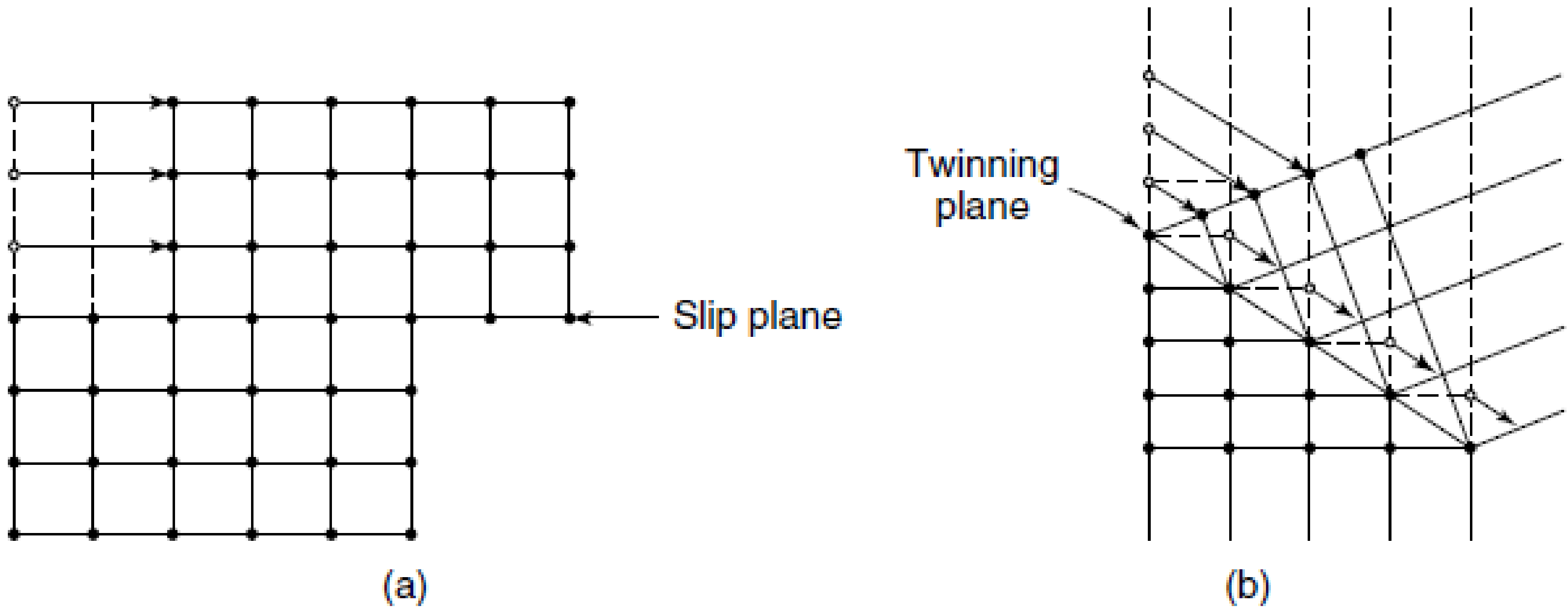

Figure 5.9 Schematic illustration of plastic deformation in single crystals by (a) slip and (b) twinning. From Z. Jastrzebski, *The Nature and Properties of Engineering Materials*, 2nd ed. Copyright © 1976 by John Wiley & Sons, Inc. This material is used by permission of John Wiley & Sons, Inc.

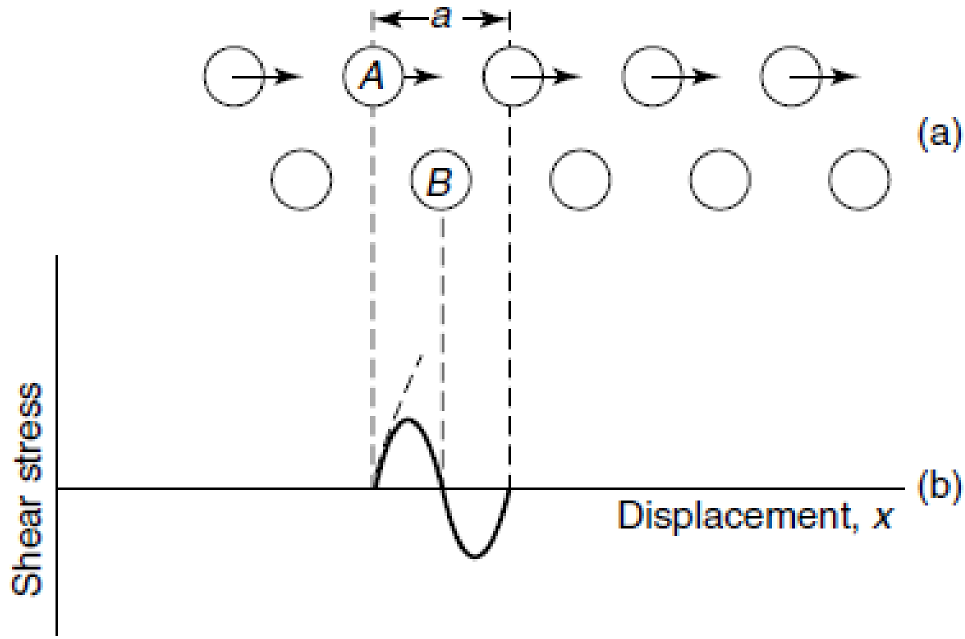

Figure 5.10 Schematic illustration of (a) relative shear of two planes of atoms in a strained material and (b) shear stress as a function of relative displacement of the planes from their equilibrium positions. Reprinted, by permission, from C. Kittel, *Introduction to Solid State Physics*, 2nd ed., p. 517. Copyright © 1957 by John Wiley & Sons, Inc.

Calculating the critical shear stress, τ_{cr}

$$\tau = G\gamma$$

$$\tau = G\frac{x}{d}$$

Approximately/ refer previous figure

Sine wave approximation
Since when atom A is directly above atom B, stress is zero

$$\tau = \frac{Ga}{2\pi d}\sin(2\pi x/a)$$

Note: Slope of sine wave is G

For small displacements, 3rd equation reduces to second

Amplitude?

$$\tau_{cr} = \frac{Ga}{2\pi d}$$

With $a \approx d$

$$\Rightarrow \tau_{cr} \approx \frac{G}{2\pi} \approx \frac{G}{6}$$

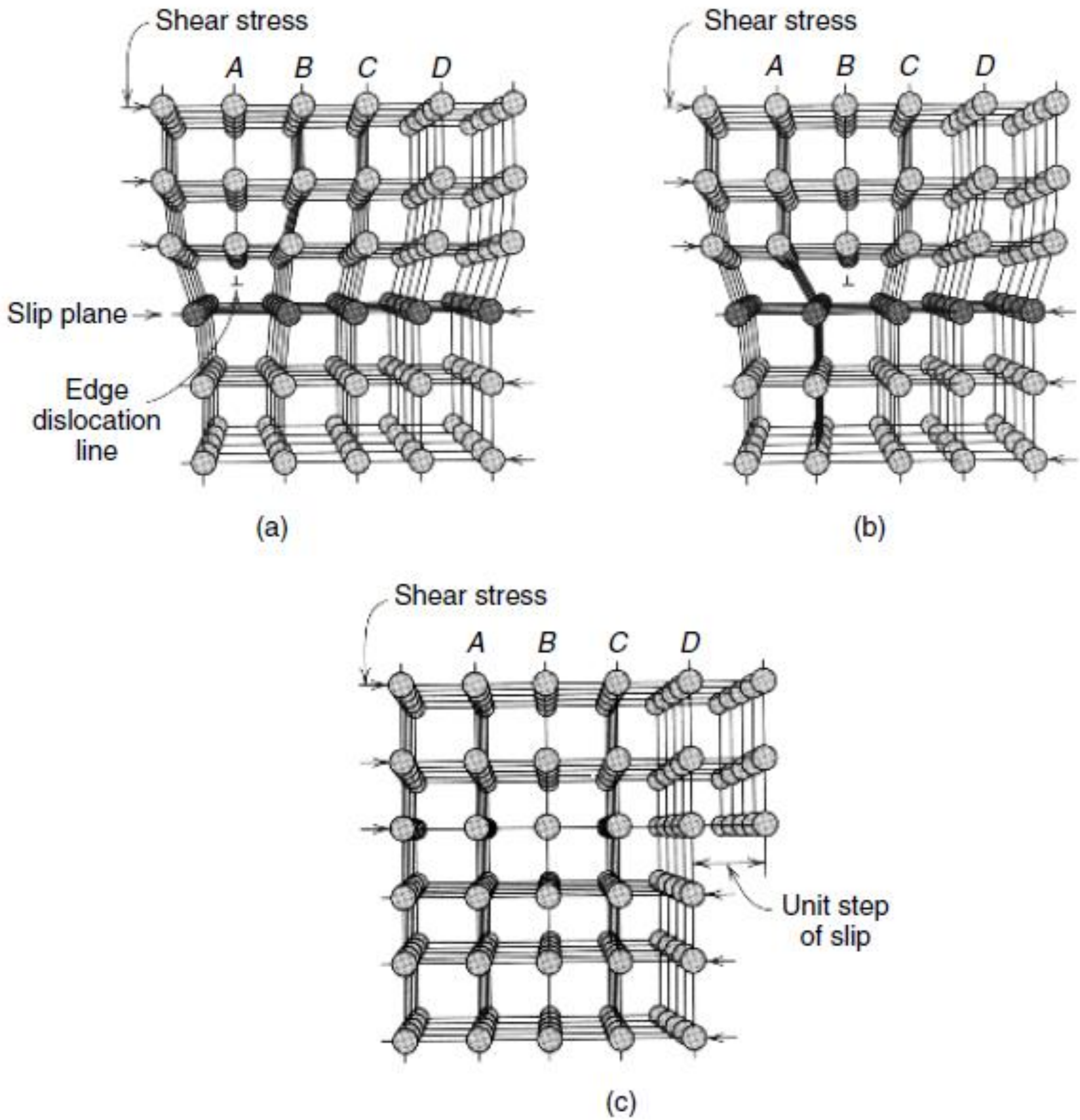

Figure 5.11 Schematic illustration edge dislocation motion in response to an applied shear stress, where (a) the extra half-plane is labeled as *A* (cf. Figure 1.28), (b) the dislocation moves one atomic distance to the right, and (c) a step forms on the crystal surface as the extra half-plane exits the crystal. Reprinted, by permission, from W. Callister, *Materials Science and Engineering: An Introduction*, 5th ed., p. 155. Copyright © 2000 by John Wiley & Sons, Inc.

Table 5.1 Slip Systems in FCC, BCC, and HCP Metals

Metals	Slip Plane	Slip Direction	Number of Slip Systems
		Face-Centered Cubic	
Cu, Al, Ni, Ag, Au	(111)	$[1\bar{1}0]$	12
		Body-Centered Cubic	
α-Fe, W, Mo	(110)	$[\bar{1}11]$	12
α-Fe, W	(211)	$[\bar{1}11]$	12
α-Fe, K	(321)	$[\bar{1}11]$	24
		Hexagonal Close-Packed	
Cd, Zn, Mg, Ti, Be	(0001)	$[11\bar{2}0]$	3
Ti, Mg, Zr	$(10\bar{1}0)$	$[11\bar{2}0]$	3
Ti, Mg	$(10\bar{1}1)$	$[11\bar{2}0]$	6

Table 5.2 Twinning Systems in FCC, BCC, and HCP Metals

Crystal Structure	Twinning Planes	Twinning Directions
fcc	(111)	$[11\bar{2}]$
bcc	(112)	$[11\bar{1}]$
hcp	$(10\bar{1}2)$	$[10\bar{1}1]$

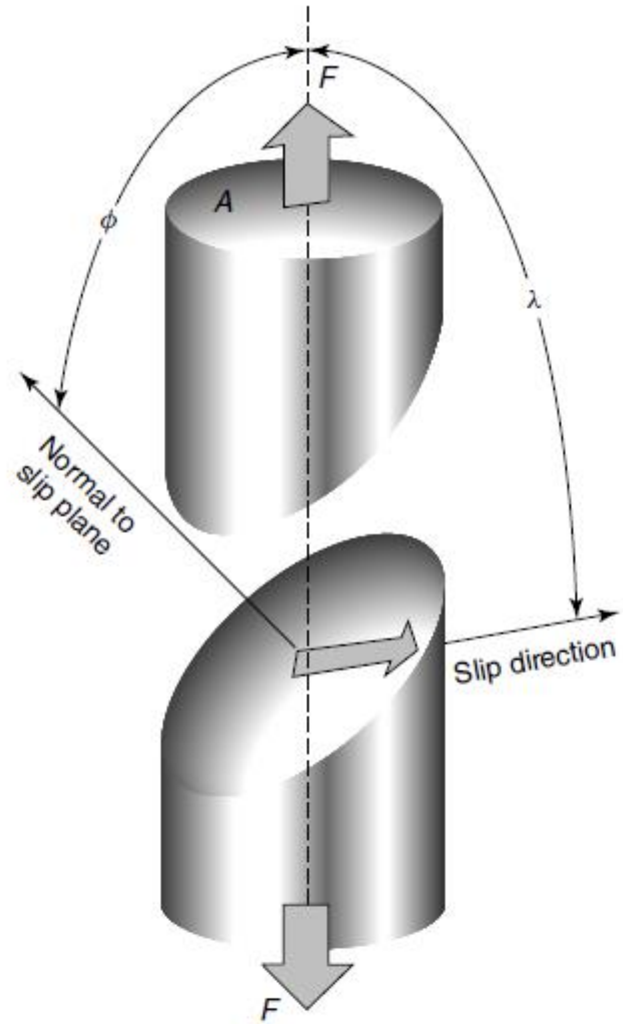

$$\phi + \lambda \neq 90°.$$

Figure 5.12 Schematic illustration of the relationship between tensile axis, slip plane, and slip direction used in calculating the resolved shear stress for a single crystal. Reprinted, by permission, from W. Callister, *Materials Science and Engineering: An Introduction*, 5th ed., p. 160. Copyright © 2000 by John Wiley & Sons, Inc.

The resolved shear stress, τ_r

$$\tau_r = \sigma_t \cos\phi \cos\lambda$$

The maximum resolved shear stress, $\tau_{r,max}$,

$$\tau_{r,\max} = \sigma_t (\cos\phi \cos\lambda)_{\max}$$

The critical resolved shear stress, τ_{cr}

$$\tau_{cr} = \sigma_{cr} (\cos\phi \cos\lambda)_{\max}$$

$$\sigma_{cr} = \sigma_y \qquad \sigma_y = \frac{\tau_{cr}}{(\cos\phi \cos\lambda)_{\max}}$$

The **minimum** stress necessary to introduce yielding

$$\sigma_y = 2\tau_{cr}$$ When $\phi = \lambda = 45^\circ$

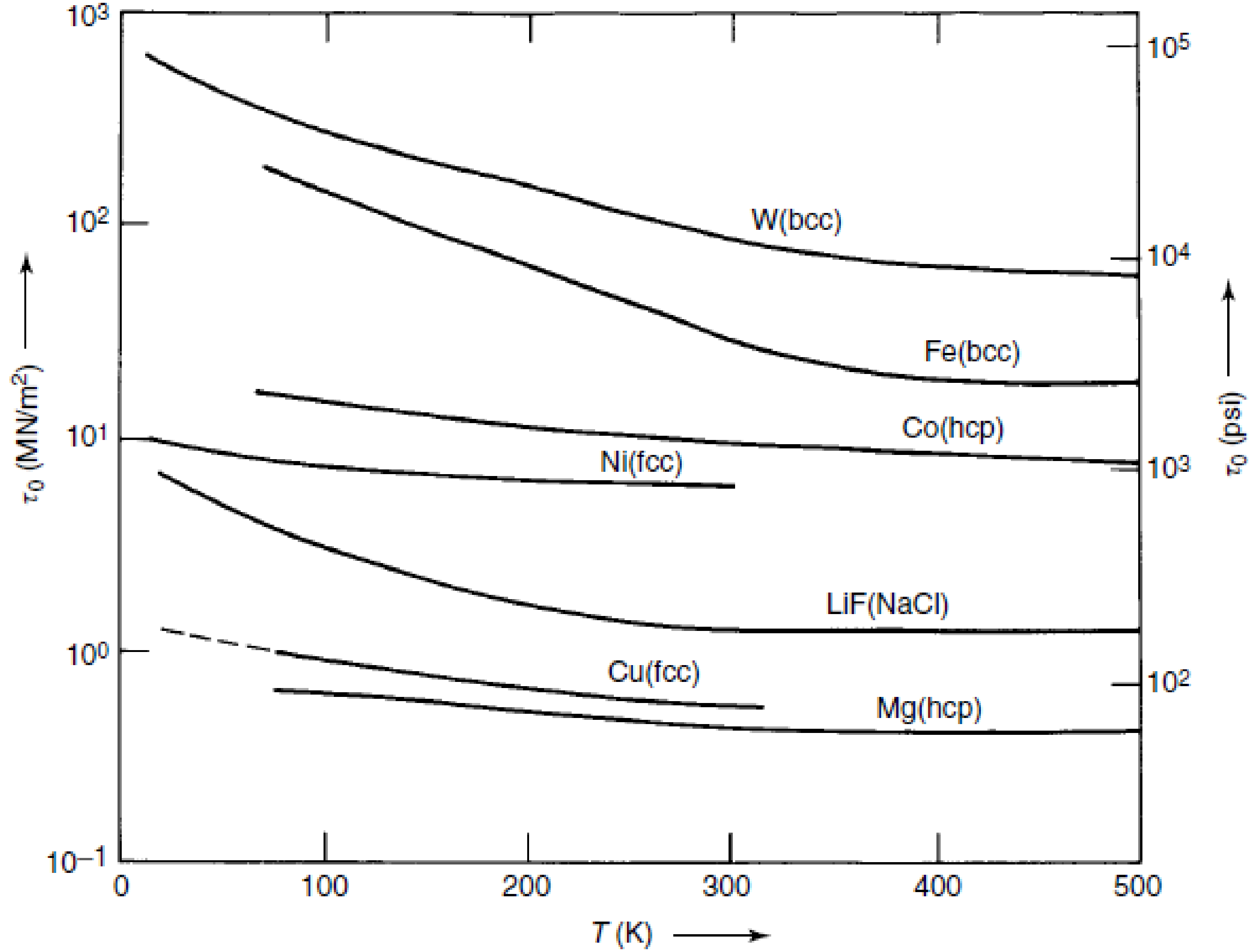

Figure 5.13 Temperature variation of critical resolved shear stress for single-crystal metals of different crystal structures. From K. M. Ralls, T. H. Courtney, and J. Wulff, *Introduction to Materials Science and Engineering*. Copyright © 1976 by John Wiley & Sons, Inc. This material is used by permission John Wiley & Sons, Inc.

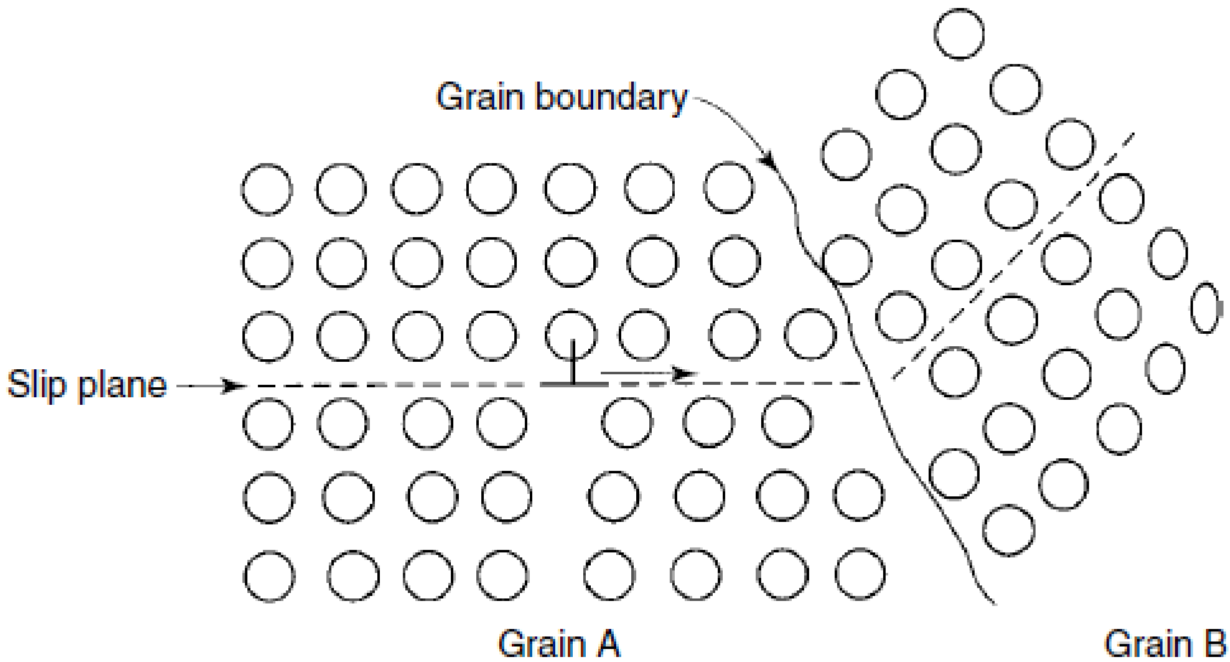

Figure 5.14 Illustration of grain boundaries acting as barriers to slip in polycrystalline materials. Reprinted, by permission, from W. Callister, *Materials Science and Engineering: An Introduction*, p. 166, 5th ed. Copyright © 2000 by John Wiley & Sons, Inc.

Hall-Petch Equation

$$\sigma_y = \sigma_0 + kd^{-1/2}$$

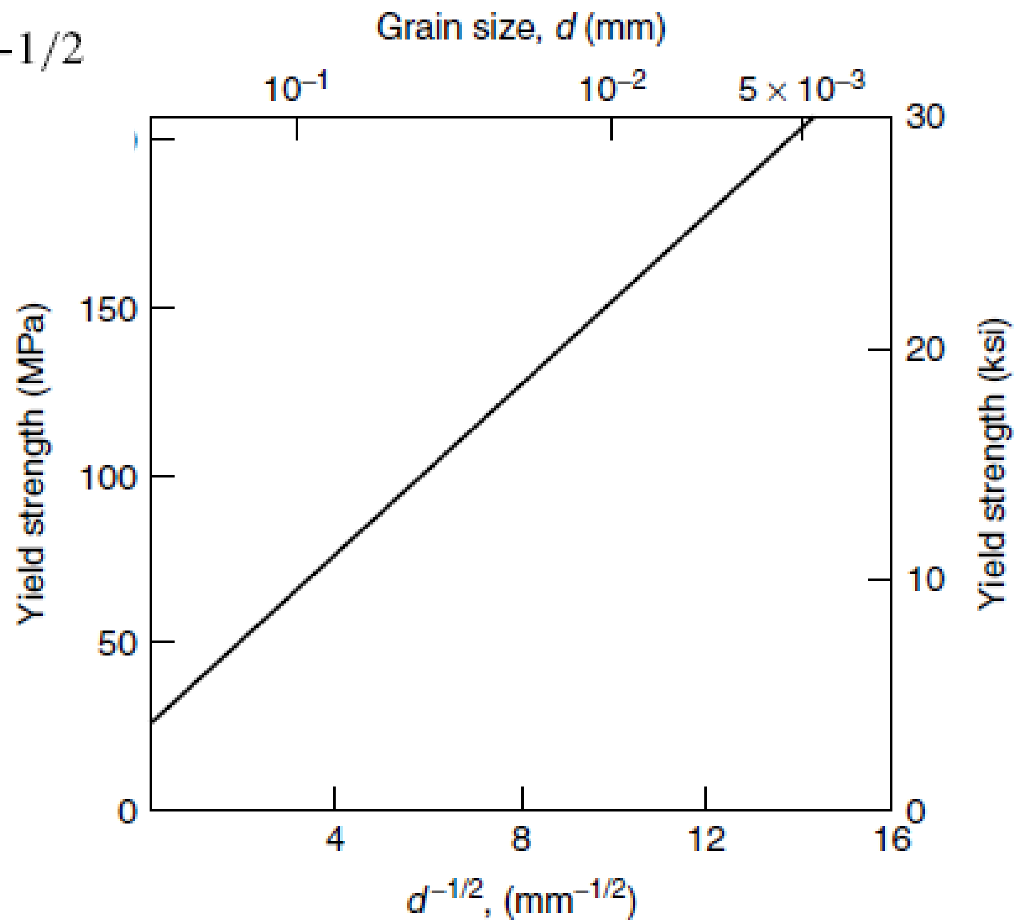

Figure 5.15 Influence of grain size on yield strength for a 70–30 Cu–Zn brass alloy. Reprinted, by permission, from W. Callister, *Materials Science and Engineering: An Introduction*, 5th ed., p. 167. Copyright © 2000 by John Wiley & Sons, Inc.

$$\tau_{cr} = \tau_{cr,0} + A\rho^{1/2}$$

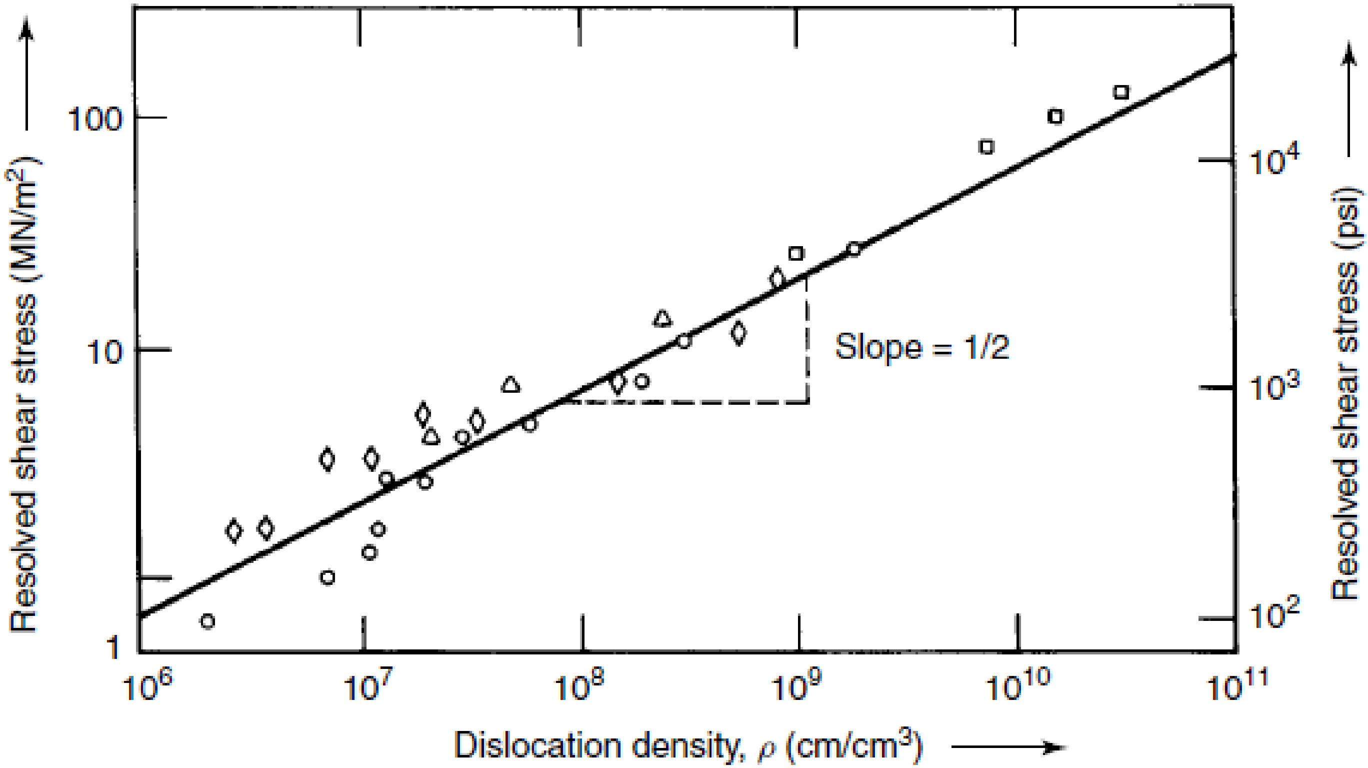

Figure 5.16 Resolved shear stress as a function of dislocation density for copper. Data are for □ polycrystalline copper; ○ single-crystal copper with one slip system operative; ◇ single-crystal copper with two slip systems operative; and △ single-crystal copper with six slip systems operative. From K. M. Ralls, T. H. Courtney, and J. Wulff, *Introduction to Materials Science and Engineering*. Copyright © 1976 by John Wiley & Sons, Inc. This material is used by permission John Wiley & Sons, Inc.

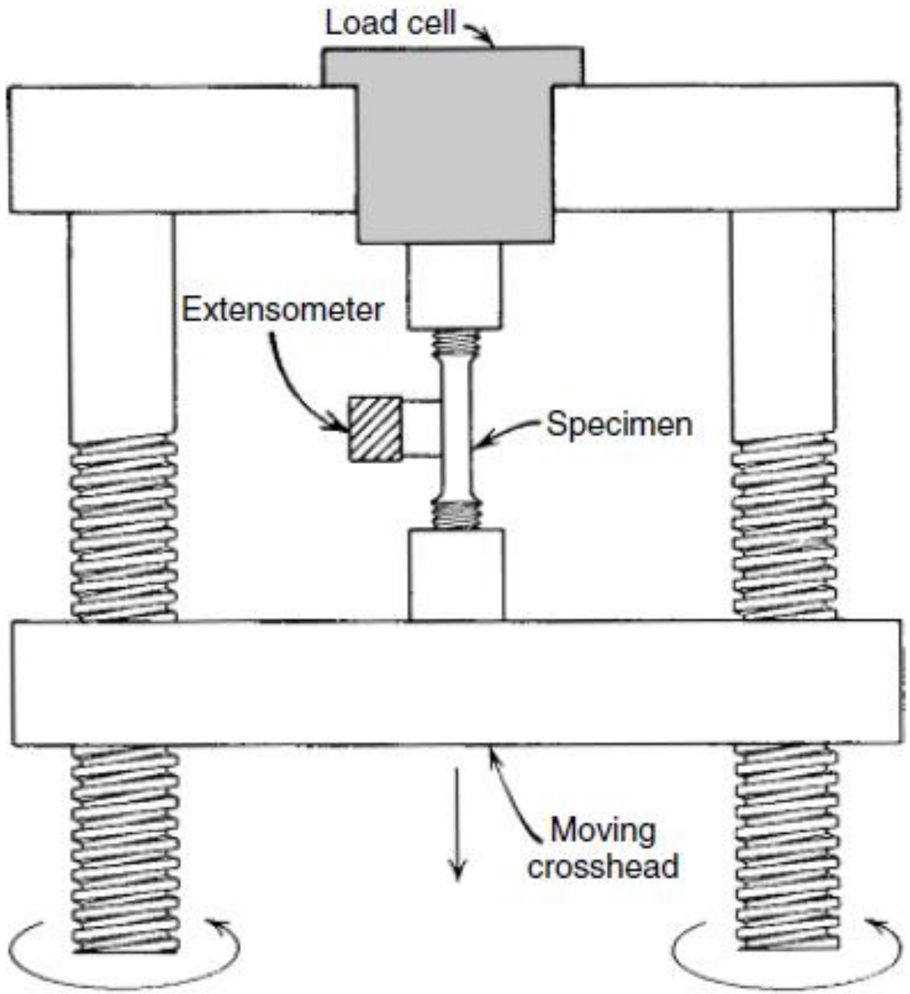

Figure 5.24 Schematic diagram of a tensile test. From K. M. Ralls, T. H. Courtney, and J. Wulff, *Introduction to Materials Science and Engineering*. Copyright © 1976 by John Wiley & Sons, Inc. This material is used by permission John Wiley & Sons, Inc.

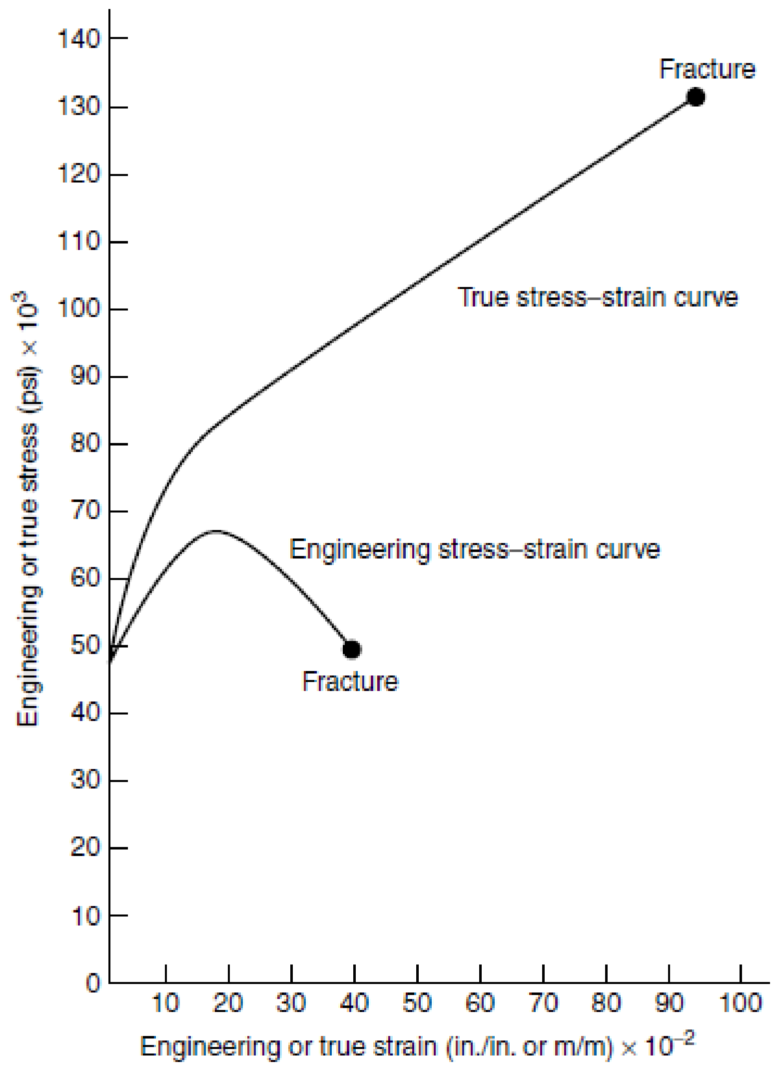

Figure 5.25 Comparison of engineering stress-engineering strain and true stress–true strain plots. Reprinted, by permission, from J. F. Shackelford, *Introduction to Materials Science for Engineers*, 5th ed., p. 192. Copyright © 2000 by Prentice Hall, Inc.

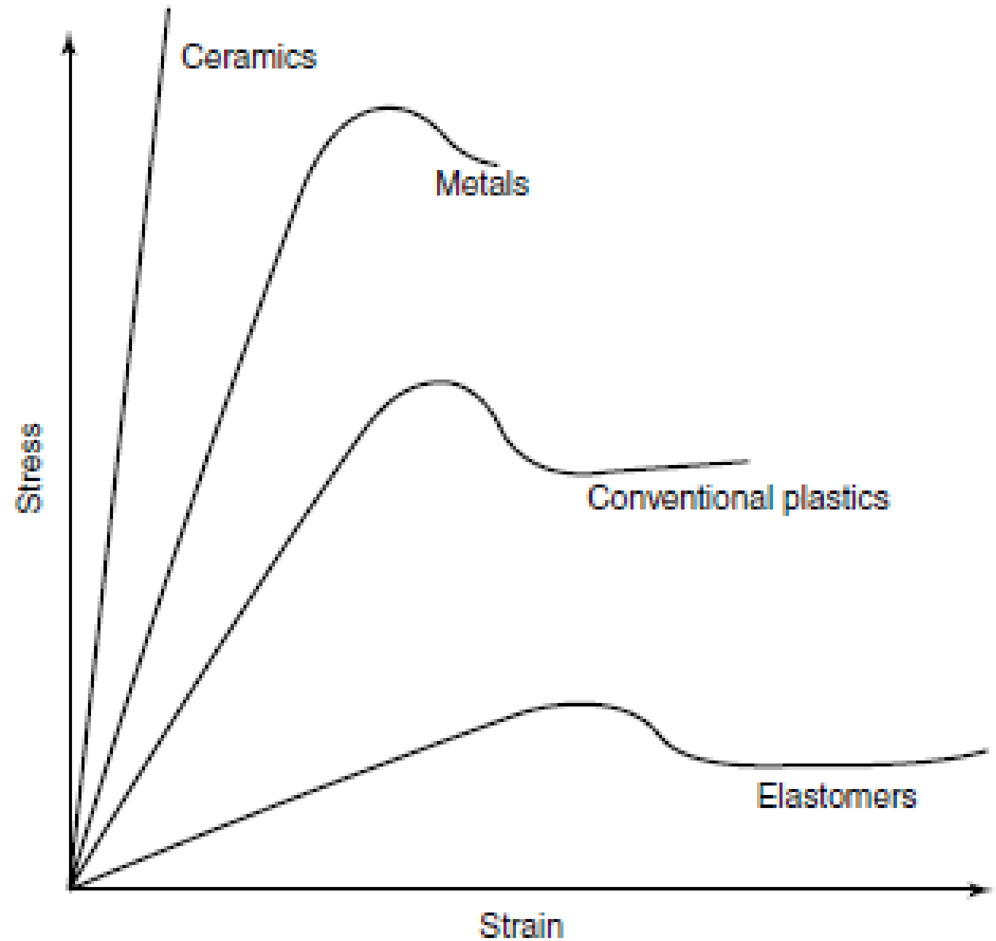

Figure 5.77 Comparison of idealized stress–strain diagrams for metals, amorphous polymers, and elastomers.

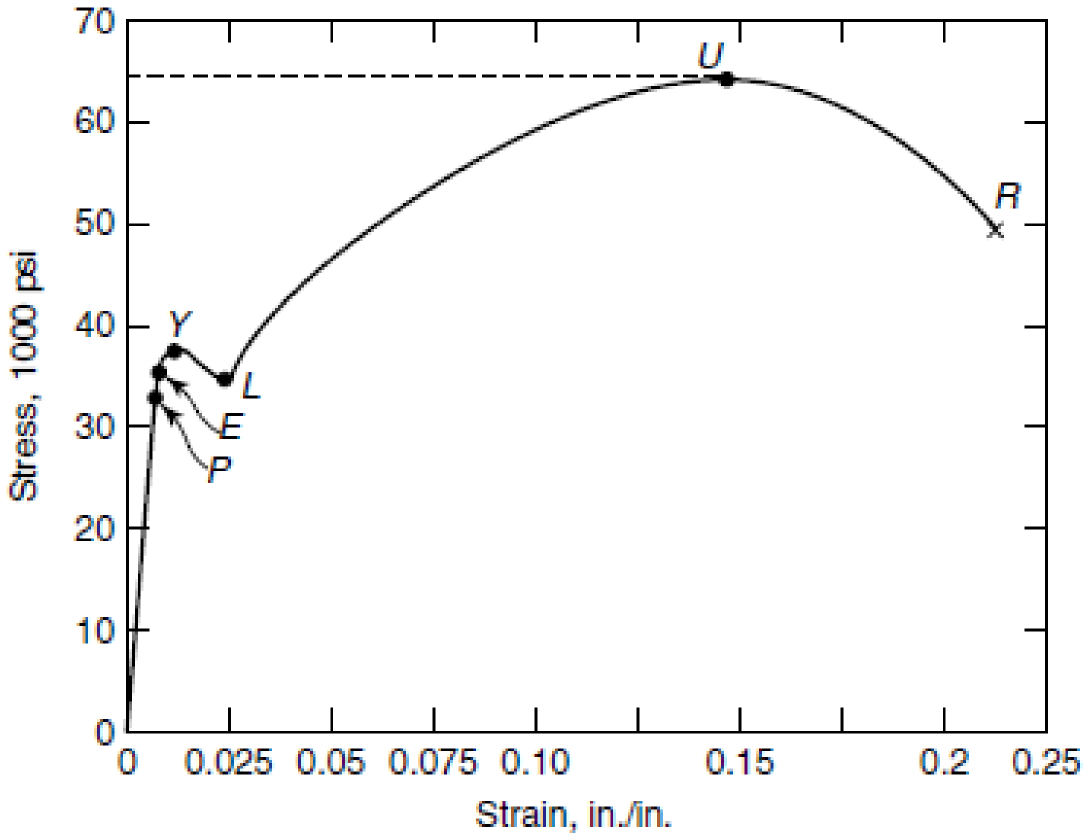

Figure 5.26 Stress–strain diagram for mild steel, illustrating different types of stress. From Z. Jastrzebski, *The Nature and Properties of Engineering Materials*, 2nd ed. Copyright © 1976 by John Wiley & Sons, Inc. This material is used by permission of John Wiley & Sons, Inc.

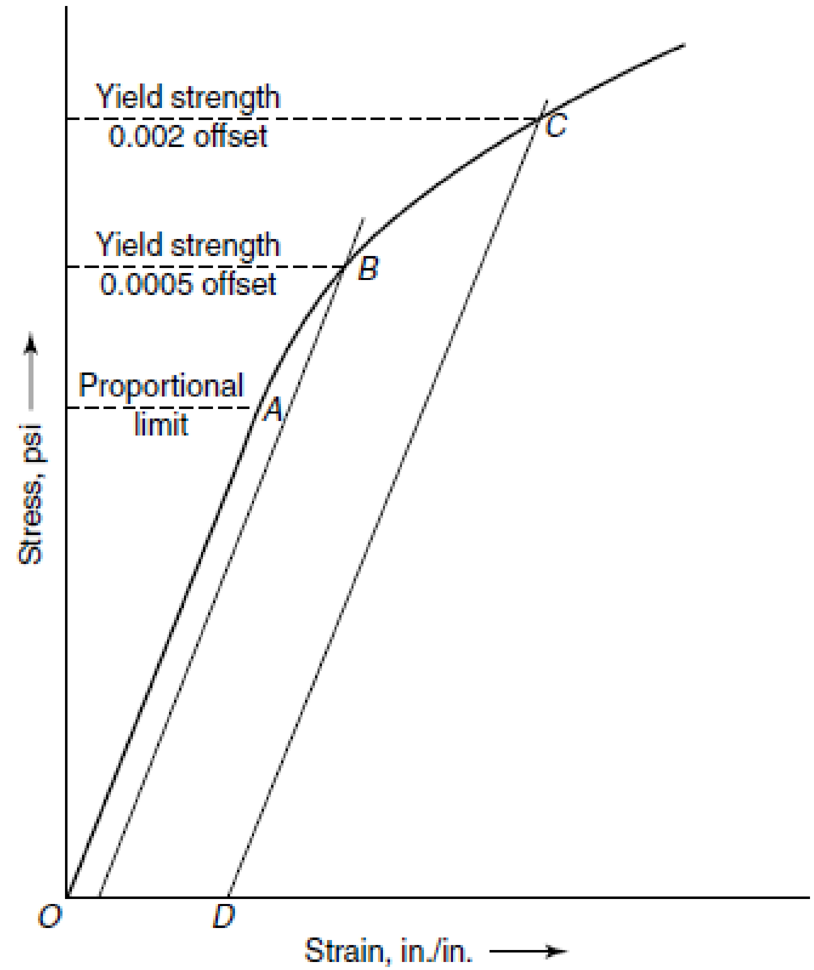

Figure 5.27 Stress–strain diagram indicating method for determining proof stress. From Z. Jastrzebski, *The Nature and Properties of Engineering Materials*, 2nd ed. Copyright © 1976 by John Wiley & Sons, Inc. This material is used by permission of John Wiley & Sons, Inc.

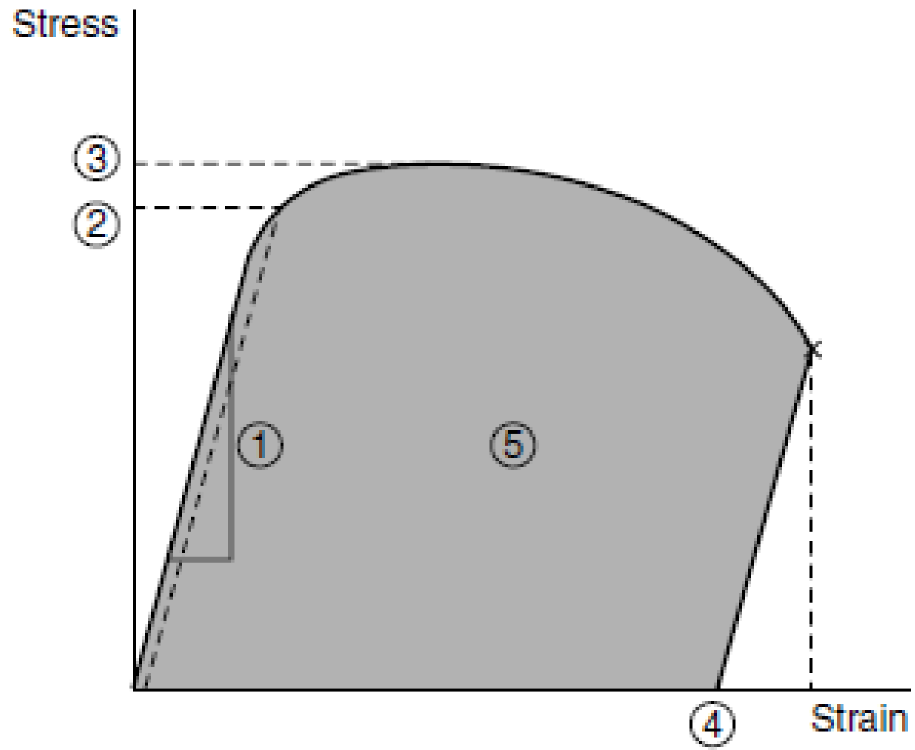

Figure 5.28 Stress–strain diagram showing (1) modulus, (2) yield strength, (3) ultimate tensile strength, (4) ductility, and (5) toughness. Note the use of proof stress in determination of yield stress. Reprinted, by permission, from J. F. Shackelford, *Introduction to Materials Science for Engineers*, 5th ed., p. 190. Copyright © 2000 by Prentice-Hall, Inc.

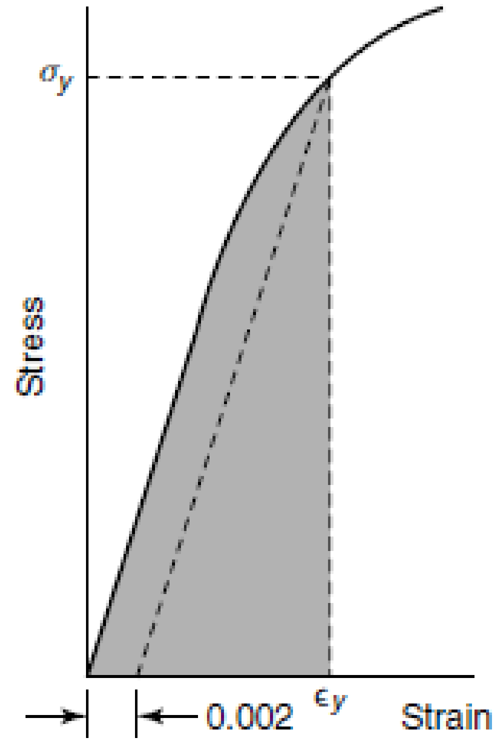

Figure 5.29 Schematic illustration of how modulus of resilience (shaded area) is determined. Reprinted, by permission, from W. Callister, *Materials Science and Engineering: An Introduction*, 5th ed., p. 130. Copyright © 2000 by John Wiley & Sons, Inc.

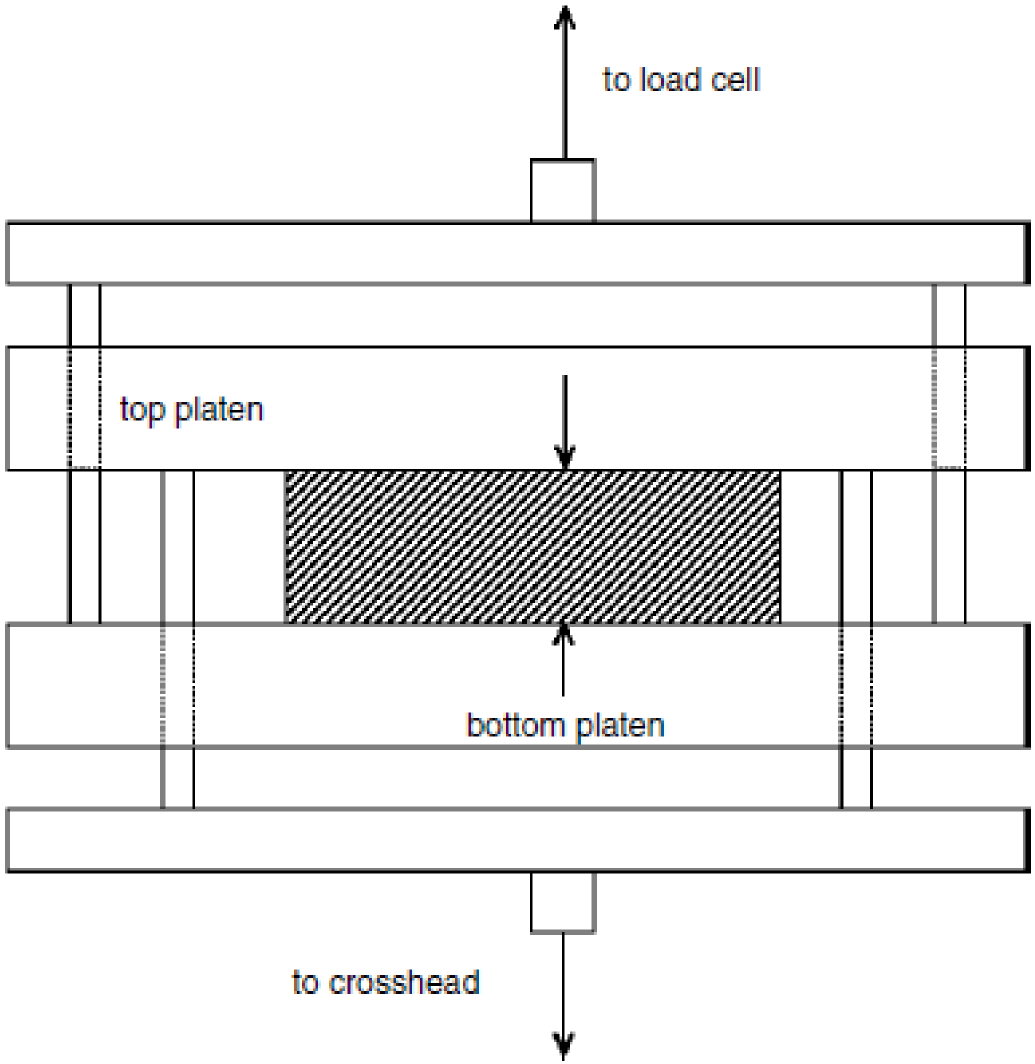

Figure 5.30 Schematic diagram of compression fixture for testing apparatus shown in Figure 5.24.

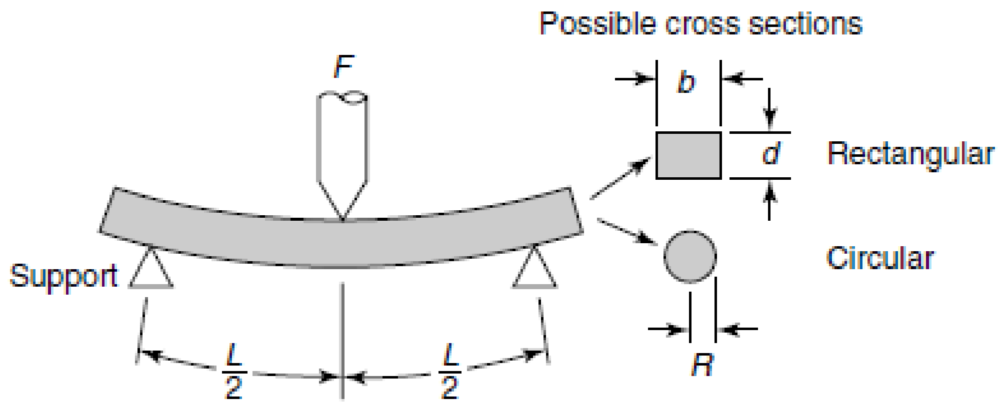

$$\sigma = \text{stress} = \frac{Mc}{I}$$

where M = maximum bending moment

c = distance from center of specimen to outer fibers

I = moment of inertia of cross section

F = applied load

	M	c	I	σ
Rectangular	$\frac{FL}{4}$	$\frac{d}{2}$	$\frac{bd^3}{12}$	$\frac{3FL}{2bd^2}$
Circular	$\frac{FL}{4}$	R	$\frac{\pi R^4}{4}$	$\frac{FL}{\pi R^3}$

Figure 5.31 Schematic illustration of a three-point bend experiment for either rectangular or circular cross sections. Reprinted, by permission, from W. Callister, *Materials Science and Engineering: An Introduction*, 5th ed., p. 409, Copyright © 2000 by John Wiley & Sons, Inc.

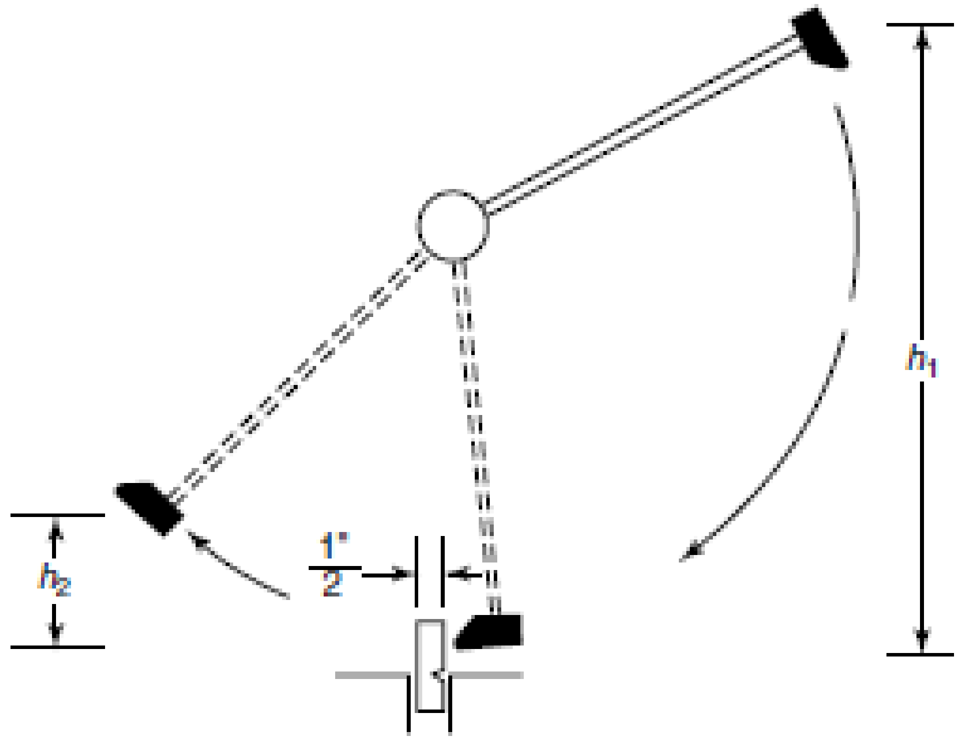

Figure 5.79 Izod (notched) impact test. Reprinted, by permission, from F. Rodriguez, *Principles of Polymer Systems*, 2nd ed., p. 235. Copyright © 1982 by Hemisphere Publishing Corporation.

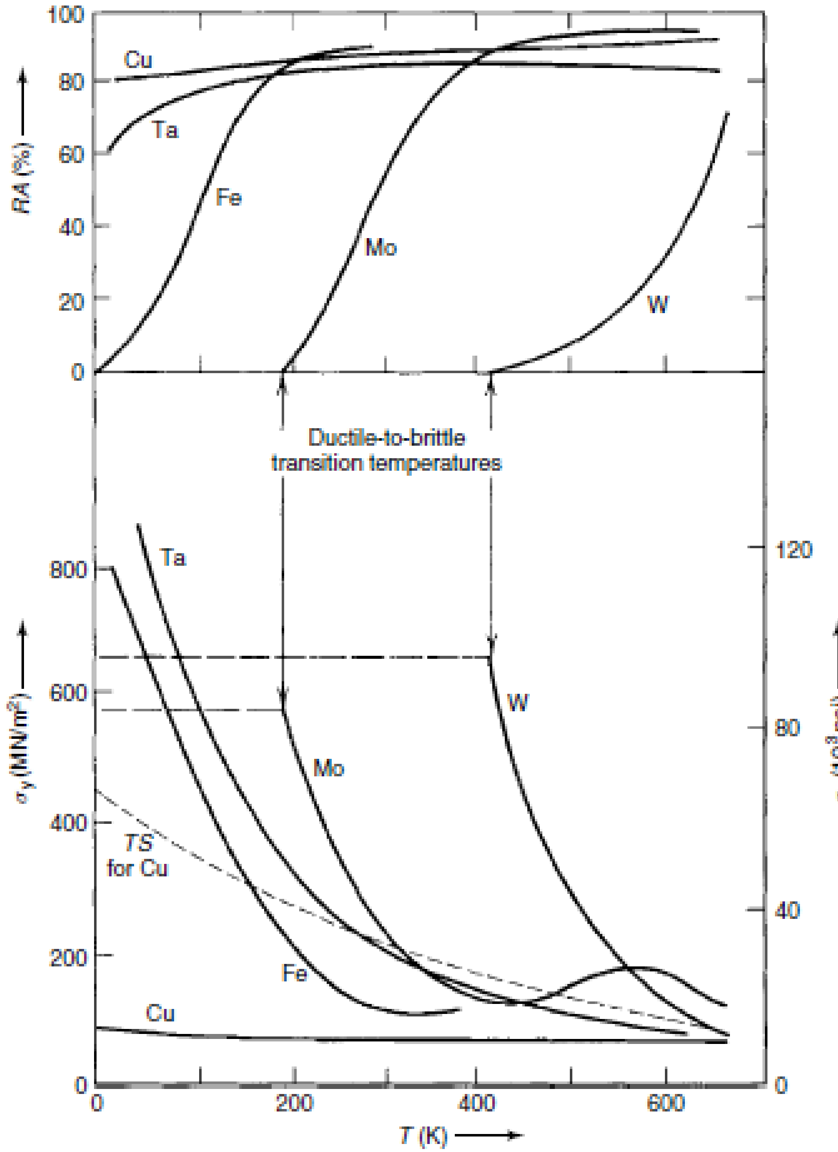

Figure 5.32 Variation of percent reduction in area (%RA, top graph) and yield strength (bottom graph) with temperature for selected metals. From K. M. Ralls, T. H. Courtney, and J. Wulff, *Introduction to Materials Science and Engineering*. Copyright © 1976 by John Wiley & Sons, Inc. This material is used by permission John Wiley & Sons, Inc.

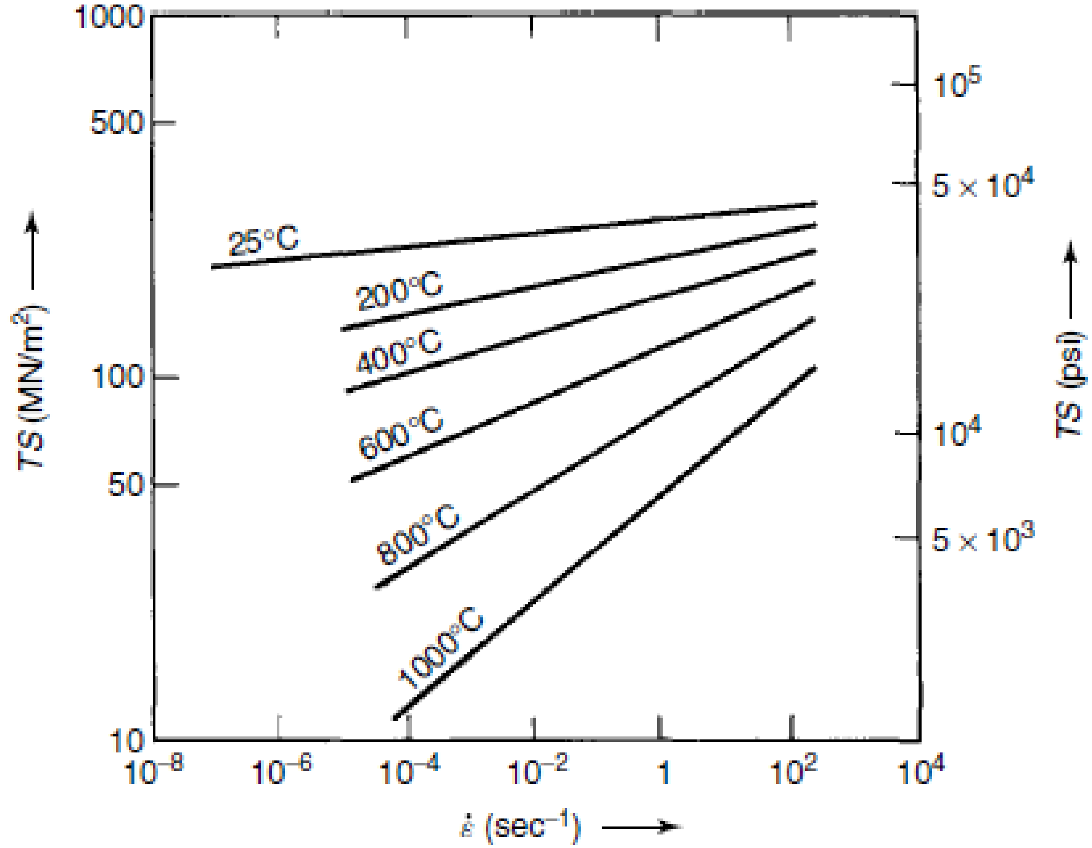

Figure 5.33 Dependence of tensile strength on strain rate and temperature for polycrystalline copper. From K. M. Ralls, T. H. Courtney, and J. Wulff, *Introduction to Materials Science and Engineering*. Copyright © 1976 by John Wiley & Sons, Inc. This material is used by permission John Wiley & Sons, Inc.

Table 5.4 Properties of Selected Alloys Exhibiting Superplasticity

Alloy Composition	Temperature of Applicability (°C)	Superplasticity (% Elongation)	*m*
	Al-Based Alloys (Balance Al)		
6%Cu–0.4%Zr–0.3%Mg	400–480	1800	0.45–0.7
5.5%Zn–2.0%Mg–1.5%Cu–0.2%Cr	510–530	1400	0.5–0.8
2.7%Cu–2.2%Li–0.7%Mg–0.12%Zr	510–530	800	0.4–0.6
4.8%Cu–1.3%Li–0.4%Mg–0.4%Ag–0.14%Zr	470–530	1000	0.45
5%Ca–5%Zn	450–550	600	0.4–0.5
4.7%Mg–0.7%Mn–0.15%Cr	480–550	670	0.4–0.65
2.5%Li–1.2%Cu–0.6%Mg–0.1%Zr	500–540	1000	0.4–0.6
	Ti-Based Alloys (Balance Ti)		
6%Al–4%V	790–940	1400	0.6–0.8
5.8%Al–4%Sn–3.5%Zr–0.5%Mo–0.3%Si–0.05%C	950–990	400	0.35–0.65
4%Al–4%Mo–2%Sn–0.5%Si	810–930	1600	0.48–0.65
4.5%Al–3%V–2%Fe–2%Mo	750–830	700	0.5–0.55
14%Al–20%Nb–3%V–2%Mo	940–980	1350	0.4–0.6
6%Al–2%Sn–4%Zr–2%Mo	880–970	900	0.5–0.7

Source: J. Pilling, Superplasticity on the Web, http://callisto.my.mtu.edu:591/FMPro?-db = sp&-format = sp.html&-view

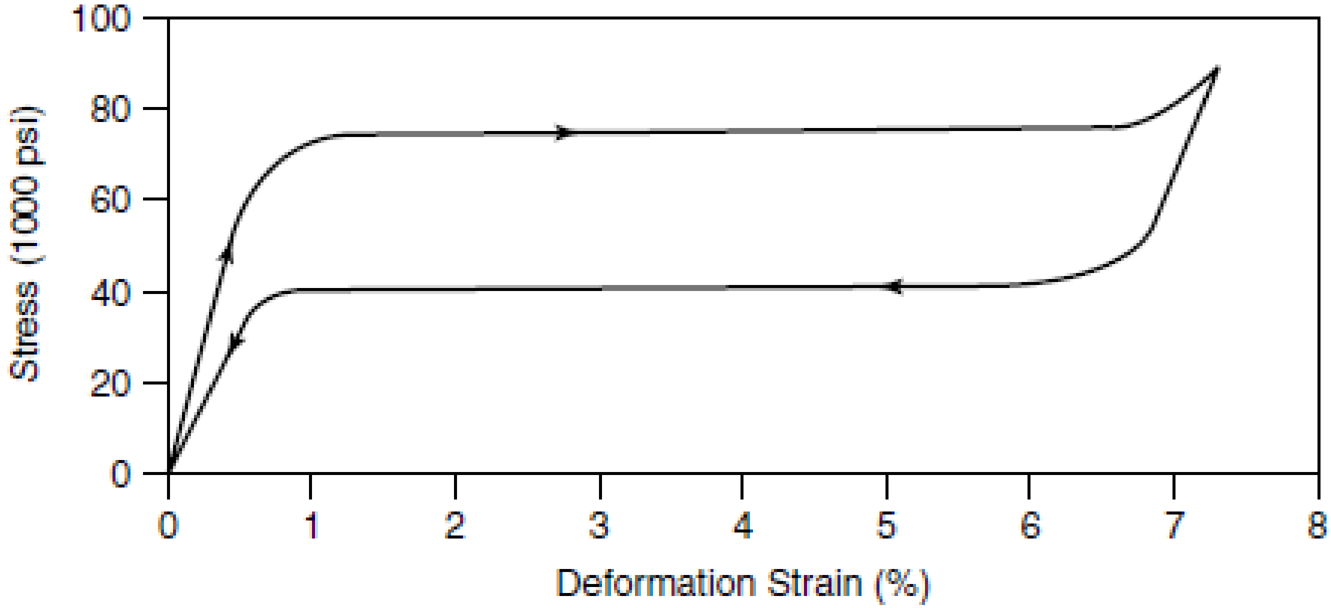

Figure 5.34 Example of superelasticity in an Ni–Ti alloy. A deformation of 7% is fully recovered. (ShapeMemory Applications, Inc.).

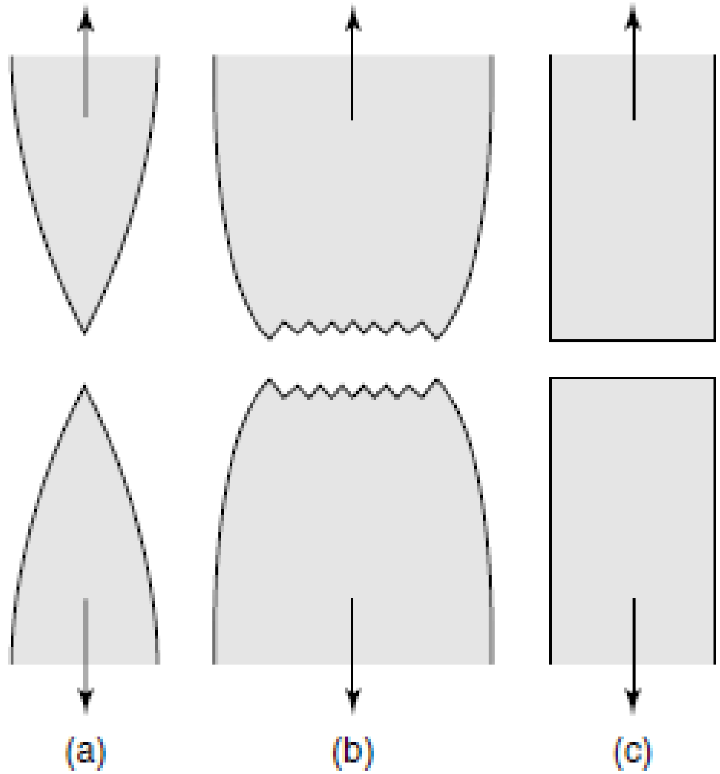

Figure 5.35 Schematic illustration of (a) rupture, (b) ductile fracture, and (c) brittle fracture. Reprinted, by permission, from W. Callister, *Materials Science and Engineering: An Introduction*, 5th ed., p. 186. Copyright © 2000 by John Wiley & Sons, Inc.

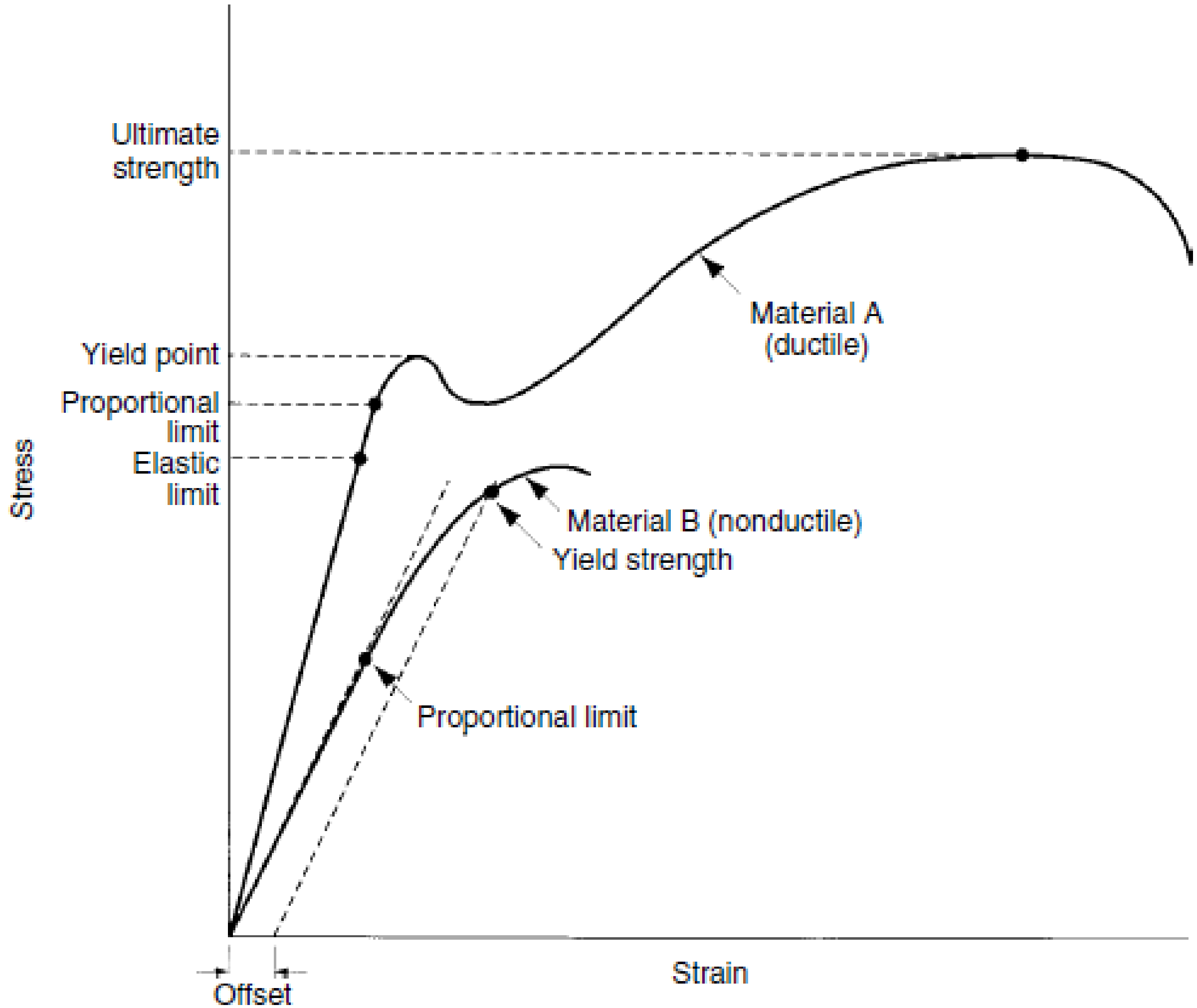

Figure 5.36 Comparison of typical stress–strain diagrams for ductile (top curve) and brittle (bottom curve) materials. Reprinted, by permission, from S. Somayaji, *Civil Engineering Materials*, 2nd ed., p. 24. Copyright © 2001 by Prentice-Hall, Inc.

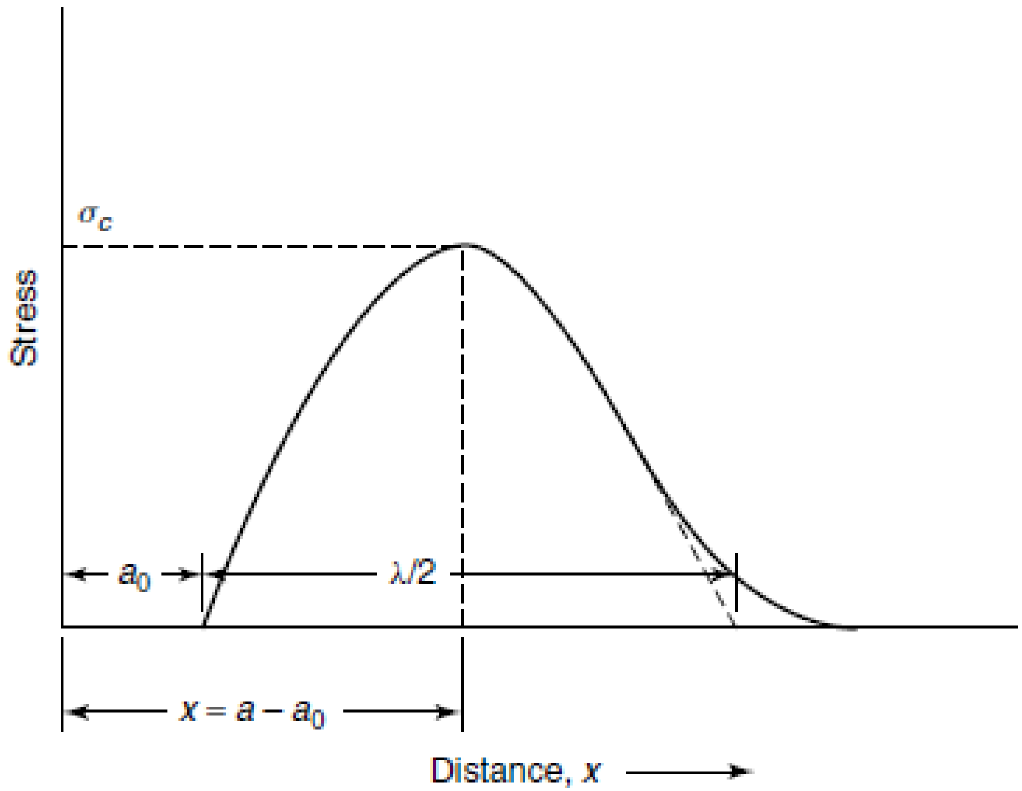

$$\sigma_c \approx \sqrt{\frac{E\gamma}{a_0}}$$

Figure 5.37 Sine-wave representation of stress variation with interatomic separation distance for two atomic planes. From Z. Jastrzebski, *The Nature and Properties of Engineering Materials*, 2nd ed. Copyright © 1976 by John Wiley & Sons, Inc. This material is used by permission of John Wiley & Sons, Inc.

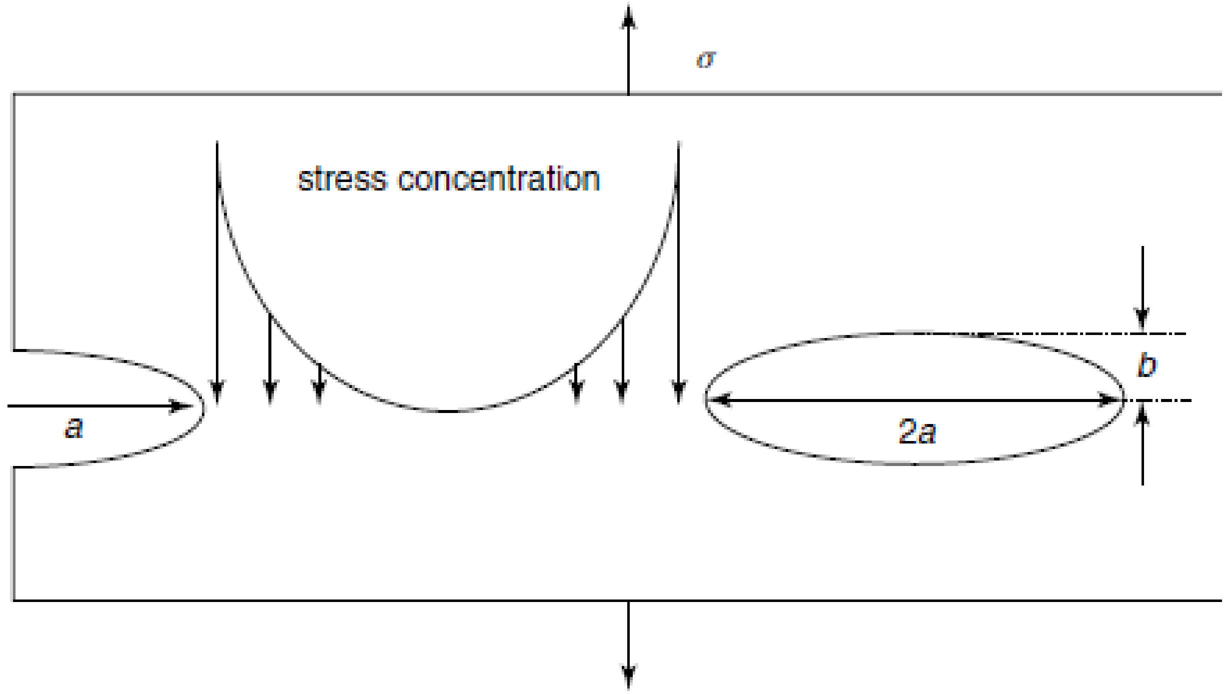

Figure 5.38 The Griffith model for micro-crack induced brittle failure. Cracks at the surface have a length of a, whereas internal cracks have a length of $2a$.

$$\sigma_m = 2\sigma_0 \left(\frac{a}{\rho}\right)^{1/2}$$

$$\sigma_f = \left(\frac{2\gamma E}{\pi a}\right)^{1/2}$$

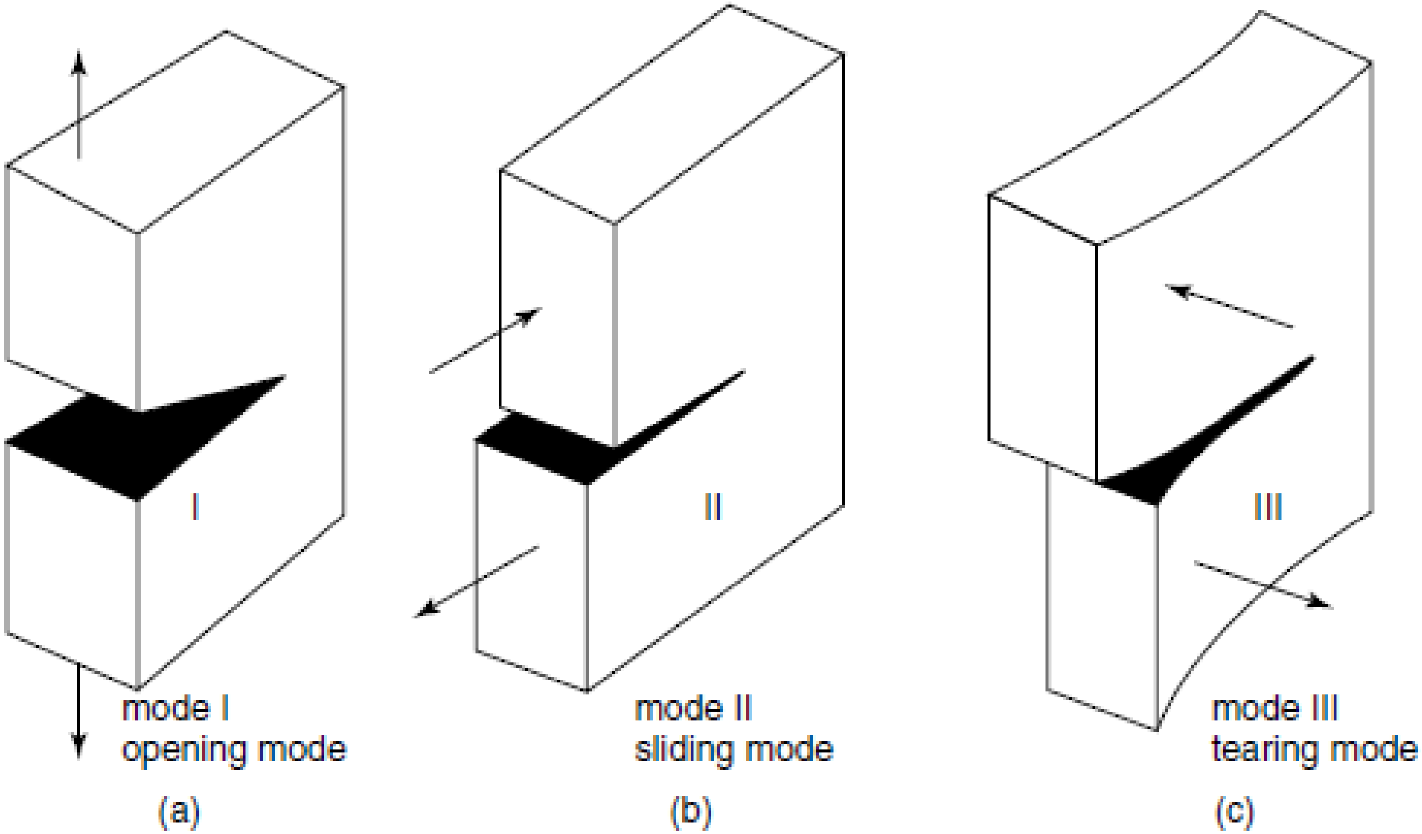

Figure 5.39 The three modes of crack surface displacement: (a) opening mode; (b) sliding mode; and (c) tearing mode.

$$K_{1c} = Y\sigma_c\sqrt{\pi a}$$

FATIGUE

Reversed
Repeating
Fluctuating
Random

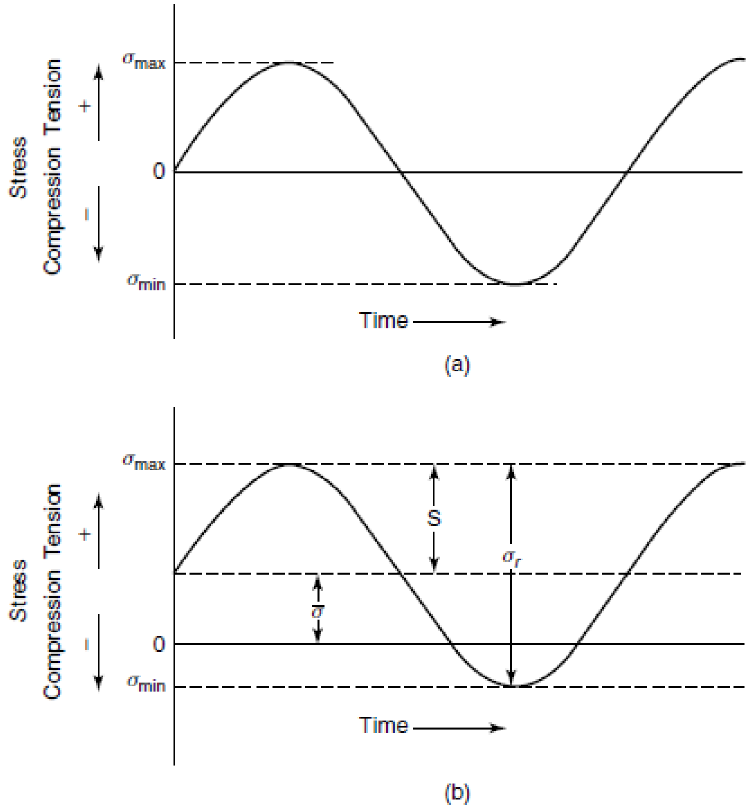

Figure 5.40 Variation of stress with time that accounts for fatigue failure by (a) a reversed stress cycle and (b) a repeated stress cycle. Reprinted, by permission, from W. Callister, *Materials Science and Engineering: An Introduction*, 5th ed., p. 210. Copyright © 2000 by John Wiley & Sons, Inc.

$$\textit{mean stress},\ \overline{\sigma} = (\sigma_{\max} + \sigma_{\min})/2$$

$$\textit{range of stress},\ \sigma_r = \sigma_{\max} - \sigma_{\min}$$

$$\textit{stress amplitude},\ S = (\sigma_{\max} - \sigma_{\min})/2$$

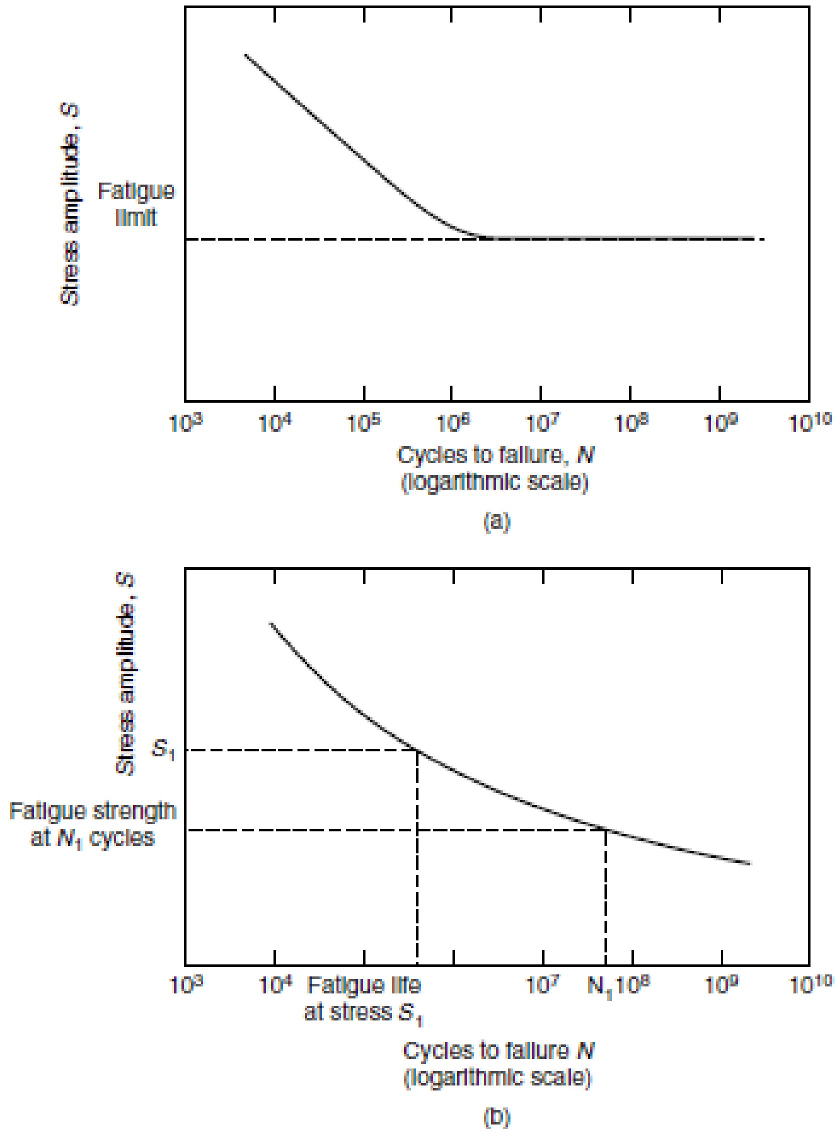

Figure 5.41 Stress amplitude versus cycles to failure illustrating (a) fatigue limit and (b) fatigue life. Reprinted, by permission, from W. Callister, *Materials Science and Engineering: An Introduction*, 5th ed., p. 212. Copyright © 2000 by John Wiley & Sons, Inc.

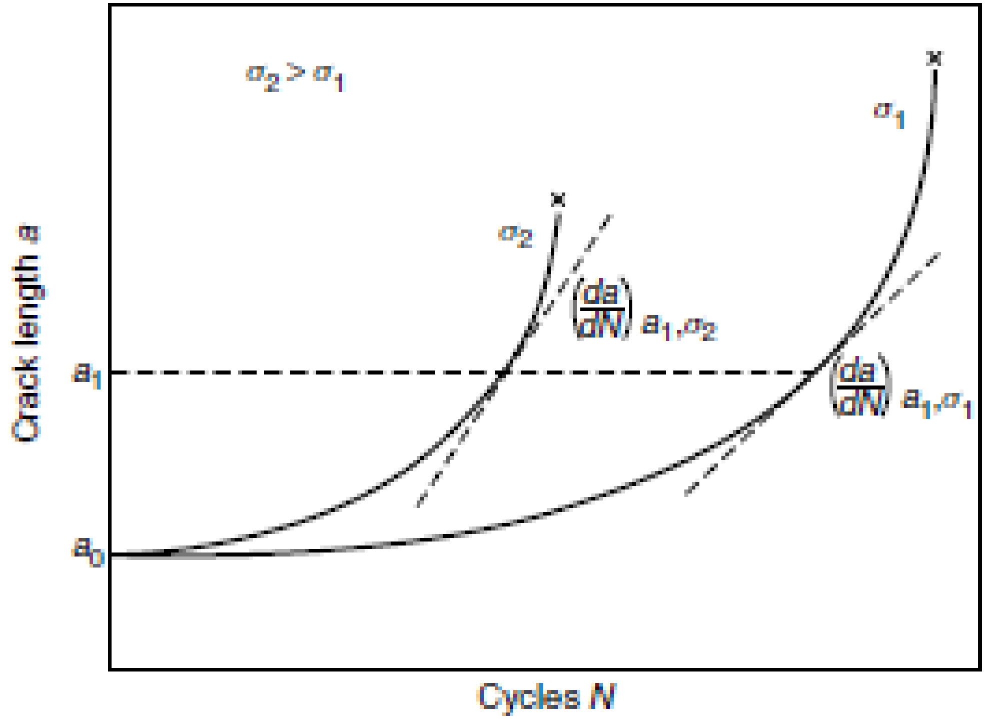

Figure 5.42 Determination of crack growth rate, *da/dN* from crack length versus number of cycles data. Reprinted, by permission, from W. Callister, *Materials Science and Engineering: An Introduction*, 5th ed., p. 217. Copyright © 2000 by John Wiley & Sons, Inc.

Paris' Equation

$$\frac{dA}{dn} = A(\Delta K)^m$$

$$\Delta K = Y(\sigma_{\max} - \sigma_{\min})\sqrt{\pi a}$$

Coffin-Manson relationship

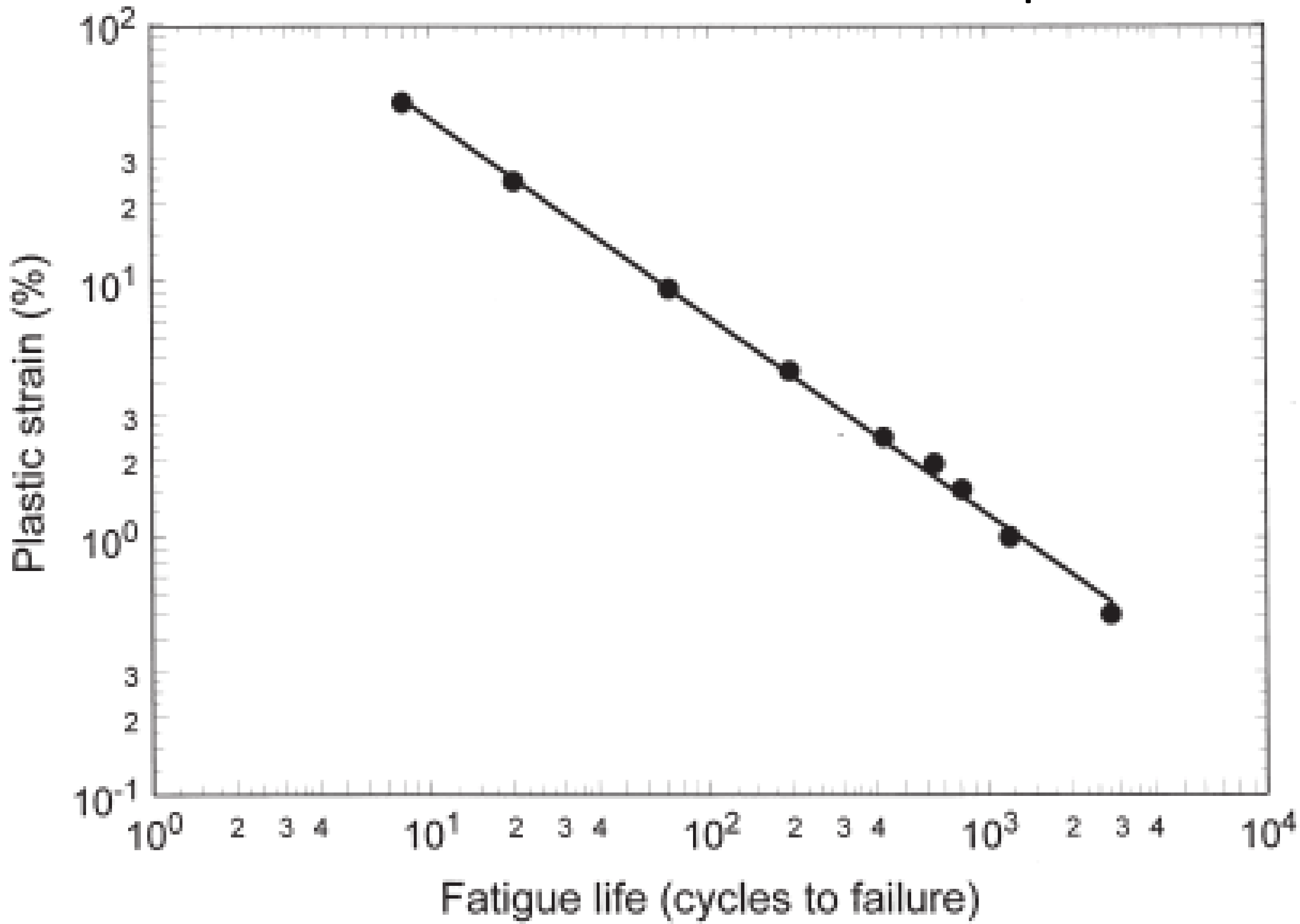

Fig. 3. Plastic strain range versus fatigue life at 25°C and 1 Hz.

$$N_f^m \Delta\varepsilon_p = C$$

N_f: Fatigue life
$\Delta\varepsilon_p$ = Plastic strain %

X.Q. Shi et al. / International Journal of Fatigue 22 (2000) 217–228

Frequency modified Coffin-Manson relationship

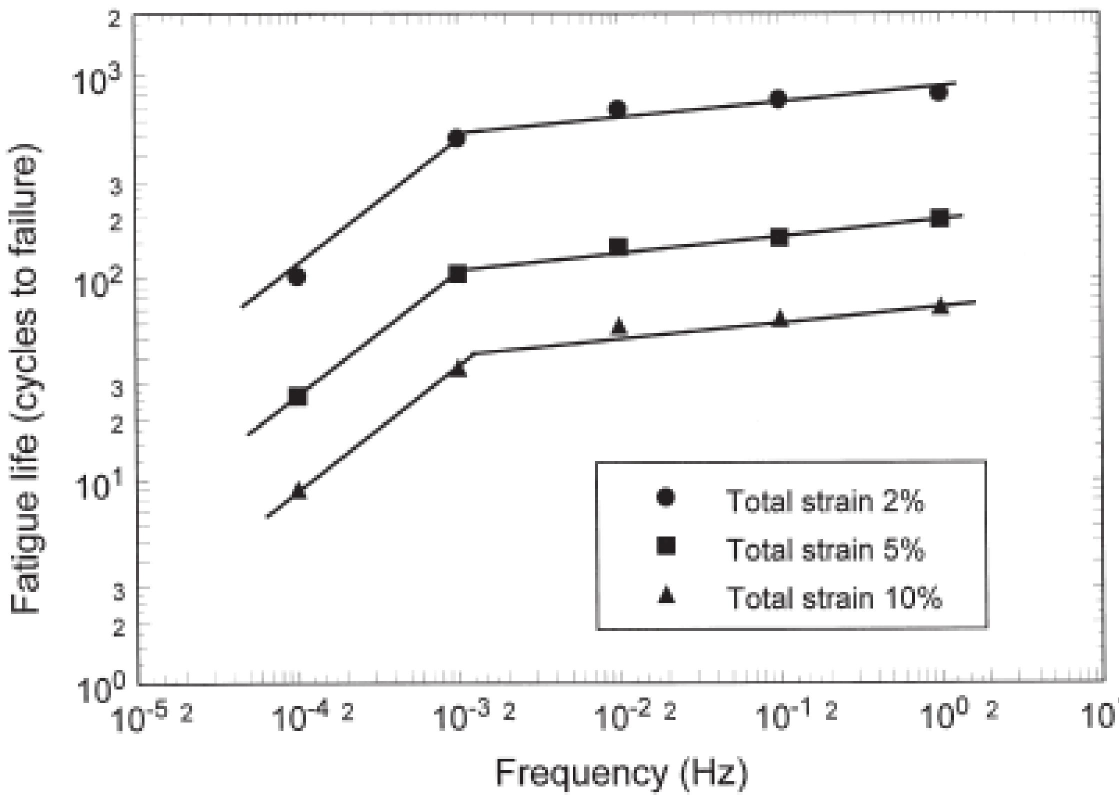

Fig. 10. Relationship between fatigue life and frequency at the temperature (25°C).

$$\left[N_f \nu^{(k-1)}\right]^m \Delta\varepsilon_p = C$$

X.Q. Shi et al. / International Journal of Fatigue 22 (2000) 217–228

Frequency Modified Paris' Equation

$$\frac{dA}{dn} = A(\Delta K)^m$$

$$\frac{dA}{dn} = C' f^{-n} (\Delta K)^m$$

YAO and SHANG: FATIGUE CRACK GROWTH IN TiB_2–SiC COMPOSITE

Acta metall. mater. Vol. 42, No. 2, pp. 589–596, 1994

CREEP

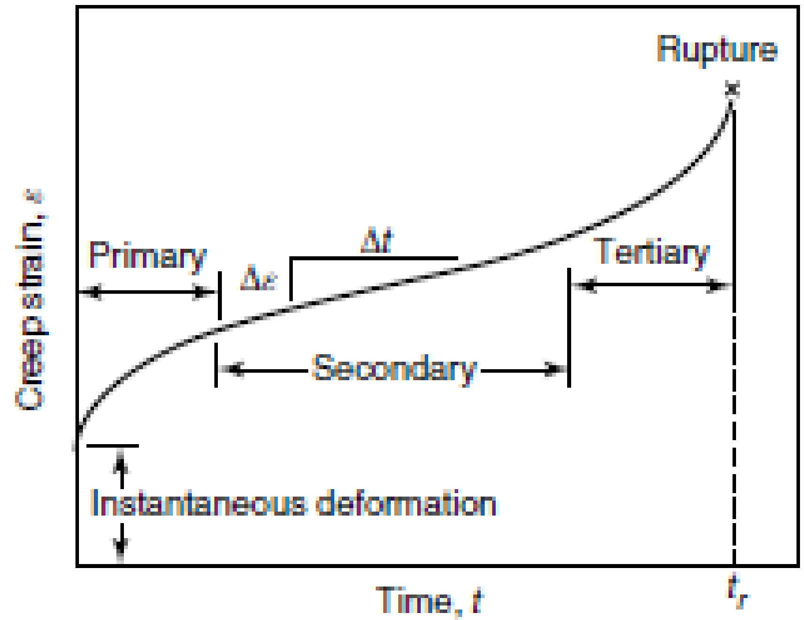

Figure 5.43 Representative creep curve illustrating primary, secondary, and tertiary creep. Reprinted, by permission, from W. Callister, *Materials Science and Engineering: An Introduction*, 5th ed., p. 226. Copyright © 2000 by John Wiley & Sons, Inc.

$$\dot{\varepsilon}_s = K\sigma^m \exp\left(\frac{-E_c}{RT}\right)$$

For Steady state creep

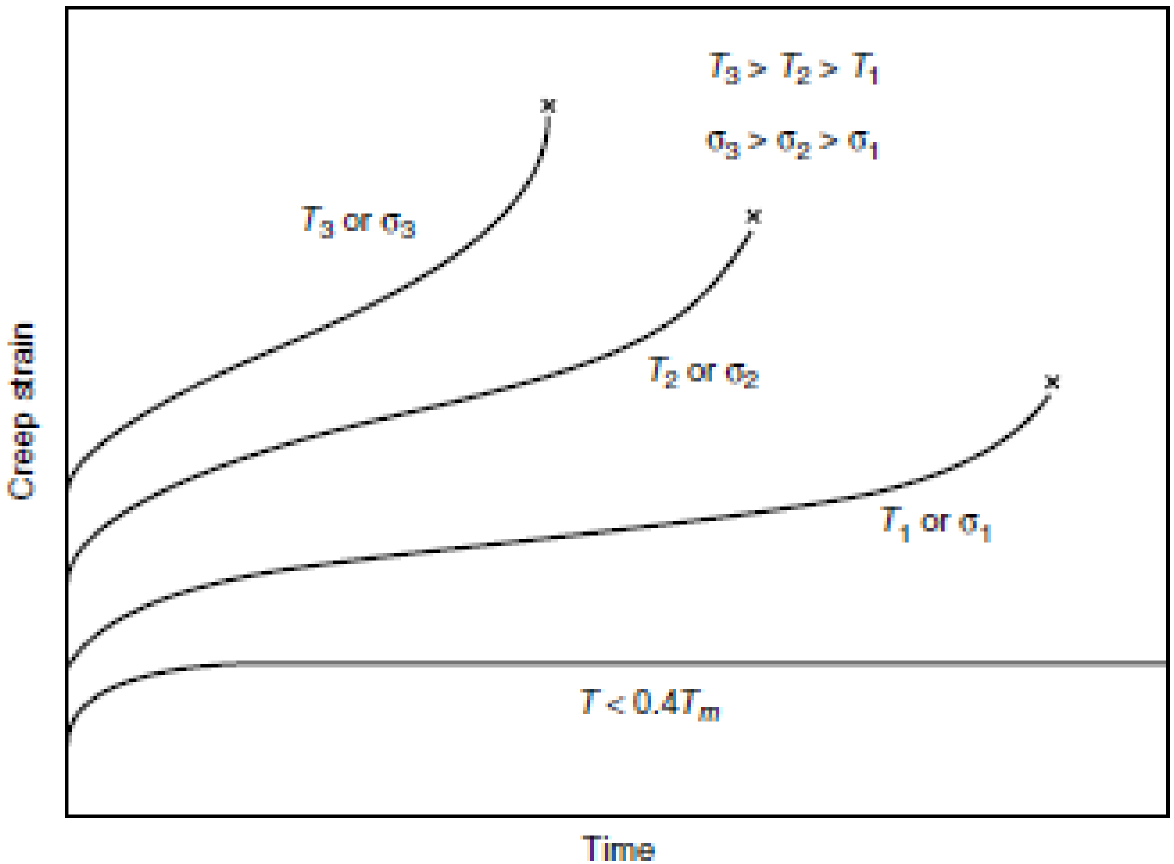

Figure 5.44 Influence of applied stress and temperature on creep behavior. Reprinted, by permission, from W. Callister, *Materials Science and Engineering: An Introduction*, 5th ed., p. 227. Copyright © 2000 by John Wiley & Sons, Inc.

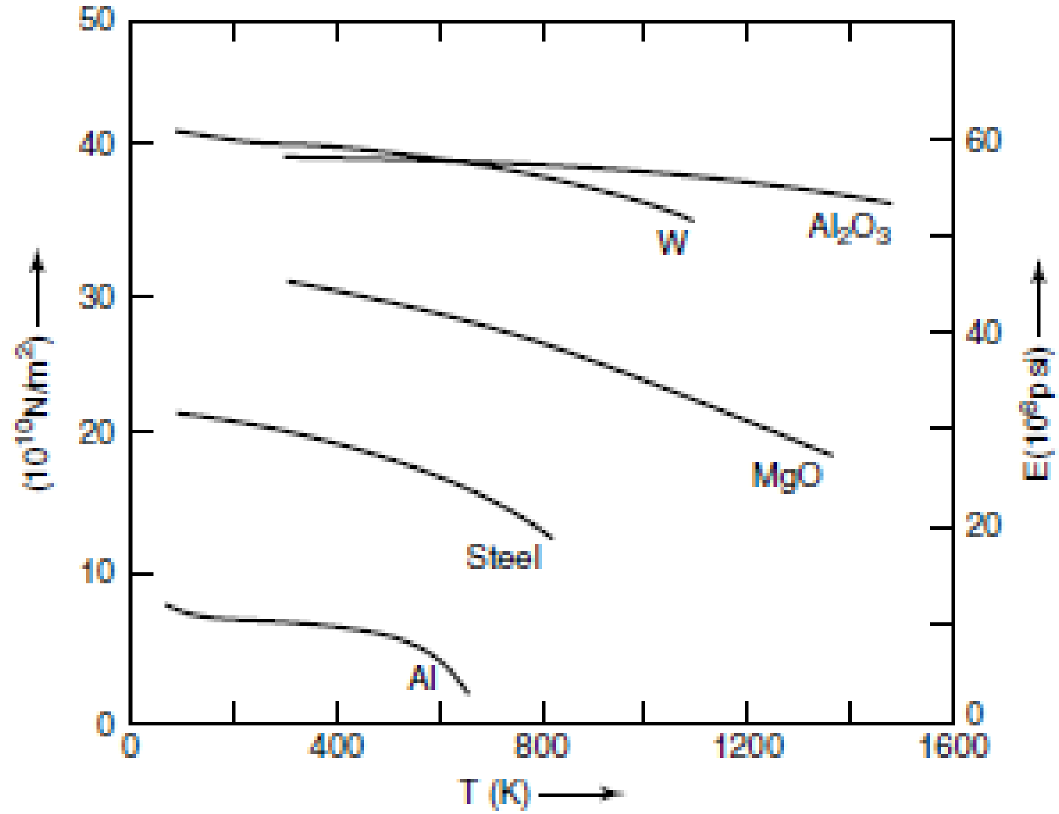

Figure 5.45 Comparison of elastic modulus between polycrystalline Al_2O_3 and some common metals as a function of temperature. From K. M. Ralls, T. H. Courtney, and J. Wulff, *Introduction to Materials Science and Engineering*. Copyright © 1976 by John Wiley & Sons, Inc. This material is used by permission John Wiley & Sons, Inc.

Table 5.5 Slip Systems in Some Ceramic Crystals

Crystal	Slip System	Number of Independent Systems	Comments
C (diamond), Si, Ge	$(111)[1\bar{1}0]$	5	At $T > 0.5T_m$
NaCl, LiF, MgO, NaF	$(110)[1\bar{1}0]$	2	At low temperatures
NaCl, LiF, MgO, NaF	$(110)[1\bar{1}0]$		At high temperatures
	$(001)[1\bar{1}0]$	5	
	$(111)[1\bar{1}0]$		
TiC, UC	$(111)[1\bar{1}0]$	5	At high temperatures
PbS, PbTe	$(001)[1\bar{1}0]$	3	
	$(110)[001]$		
CaF_2, UO_2	$(001)[1\bar{1}0]$	3	
CaF_2, UO_2	$(001)[1\bar{1}0]$		At high temperatures
	(110)	5	
	(111)		
C (graphite), Al_2O_3, BeO	$(0001)[11\bar{2}0]$	2	
TiO_2	$(101)[10\bar{1}]$	4	
	$(110)[001]$		
$MgAl_2O_4$	$(111)[1\bar{1}0]$	5	
	(110)		

Source: W. D. Kingery, H. K. Bowen and D. R. Uhlmann, *Introduction to Ceramics*. Copyright © 1976 by John Wiley & Sons, Inc.

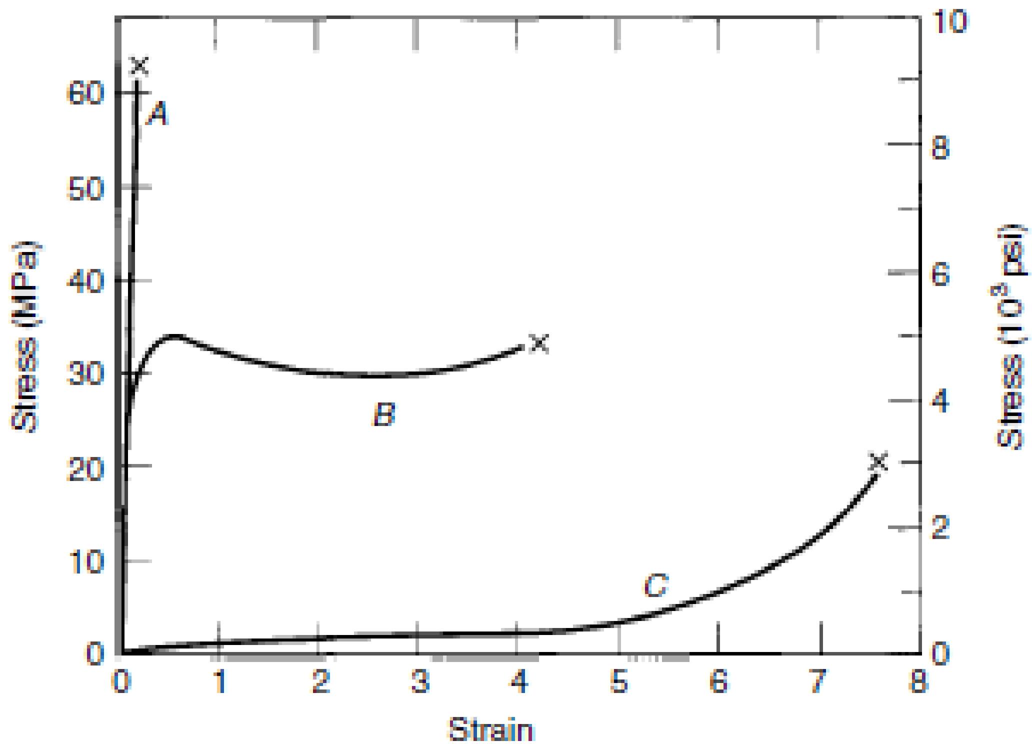

Figure 5.58 The stress–strain behavior of brittle polymer (curve A), ductile polymer (curve B), and highly elastic polymer (curve C). Reprinted, by permission, from W. Callister, *Materials Science and Engineering: An Introduction*, 5th ed., p. 475. Copyright © 2000 by John Wiley & Sons, Inc.

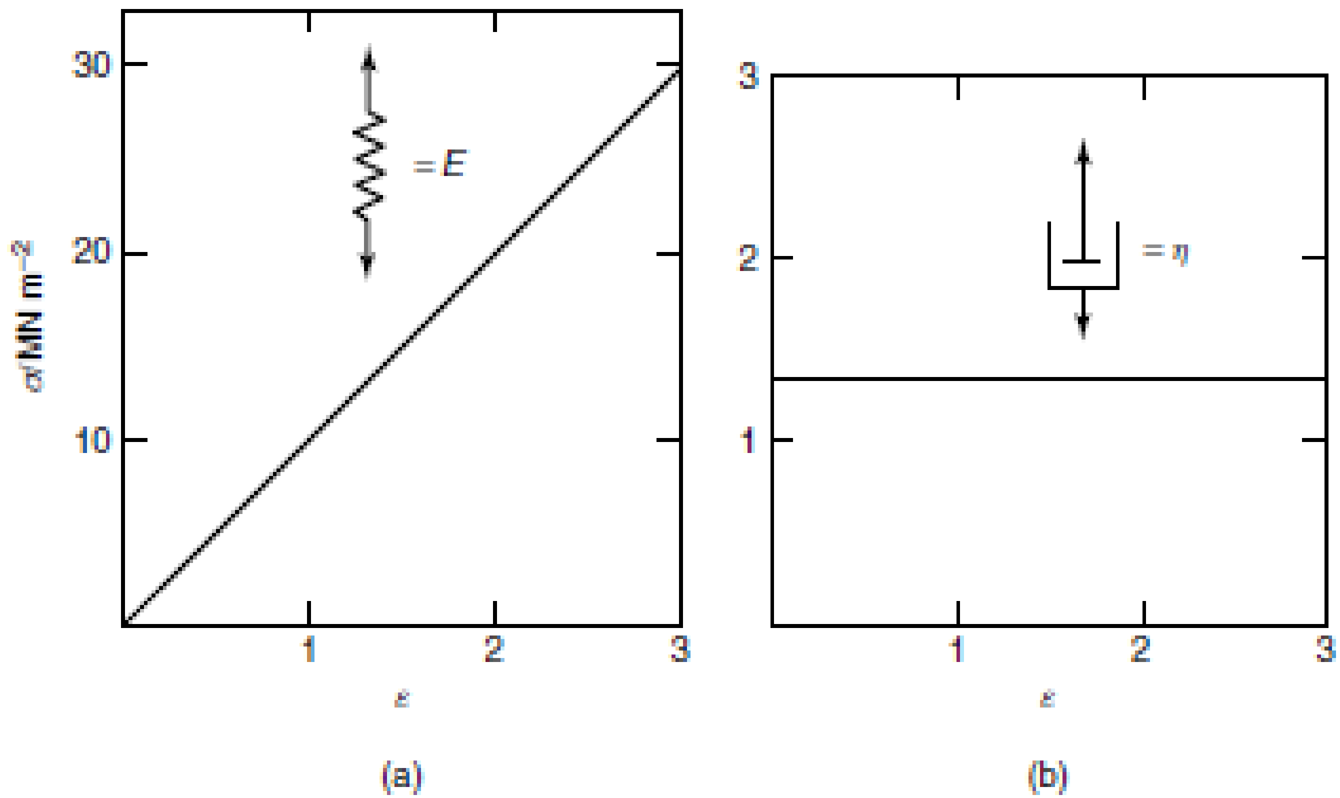

Figure 5.59 Stress–strain behavior of (a) spring of modulus E and (b) dashpot of viscosity η. Reprinted, by permission, from J. M. G. Cowie, *Polymers: Chemistry & Physics of Modern Materials*, p. 277, 2nd ed. Copyright © 1991 by J. M. G. Cowie.

Maxwell Model

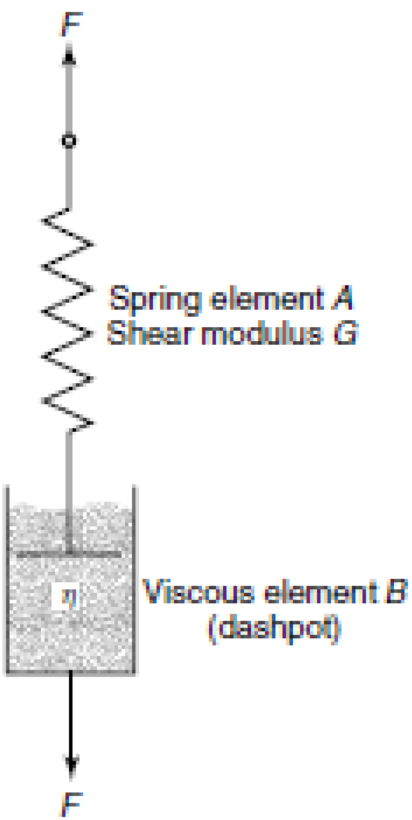

$$\tau = \tau_e = \tau_v \qquad \gamma = \gamma_e + \gamma_v$$

Missing in book

$$\dot{\gamma} = d\gamma/dt \qquad \frac{d\gamma}{dt} = \frac{d\gamma_e}{dt} + \frac{d\gamma_v}{dt}$$

Recall $\tau_e = G\gamma_e$

Differentiating and solving for strain rate:

$$\frac{d\gamma_e}{dt} = \frac{d\tau_e/dt}{G}$$

From Newton's Law of Viscosity $\tau_v = \eta \frac{d\gamma_v}{dt}$

$$\boxed{\frac{d\gamma}{dt} = \frac{1}{G}\frac{d\tau_e}{dt} + \frac{1}{\eta}\tau_v}$$

For constant shear $d\gamma/dt = 0$ $\quad \tau = \tau_0 \text{ at } t = 0 \quad \tau = \tau \text{ at } t = t$

$$\tau = \tau_0 \exp\left(\frac{-Gt}{\eta}\right) \qquad \tau = \tau_0 \exp\left(\frac{-t}{t_{rel}}\right)$$

$$t_{rel} = \eta/G$$

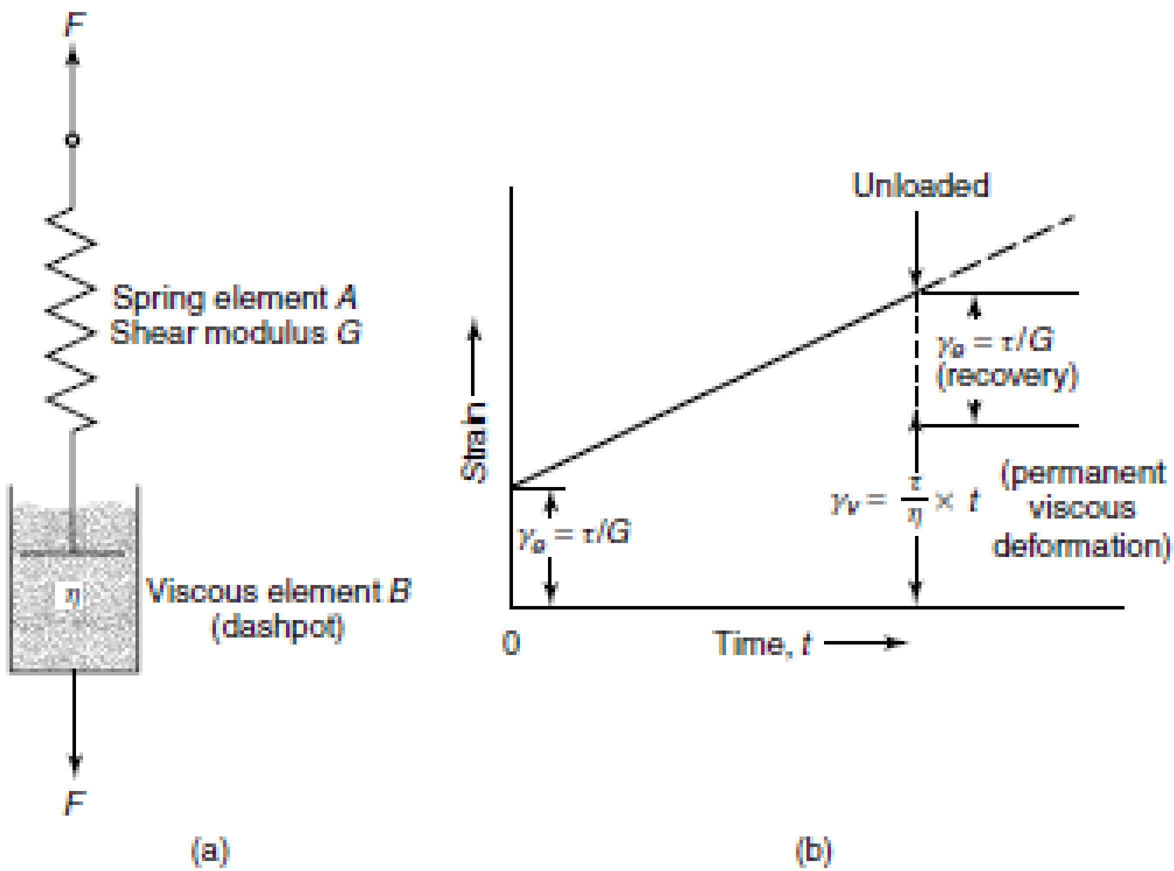

Figure 5.60 (a) Maxwell spring and dashpot in series model of viscoelasticity and (b) constant stress conditions resulting in time-dependent strain. From Z. Jastrzebski, *The Nature and Properties of Engineering Materials*, 2nd ed. Copyright © 1976 by John Wiley & Sons, Inc. This material is used by permission of John Wiley & Sons, Inc.

$$\gamma = \gamma_e = \gamma_v \qquad \tau = \tau_e + \tau_v$$

Kelvin-Voigt model

Substituting Hooke's law and Newton's Law

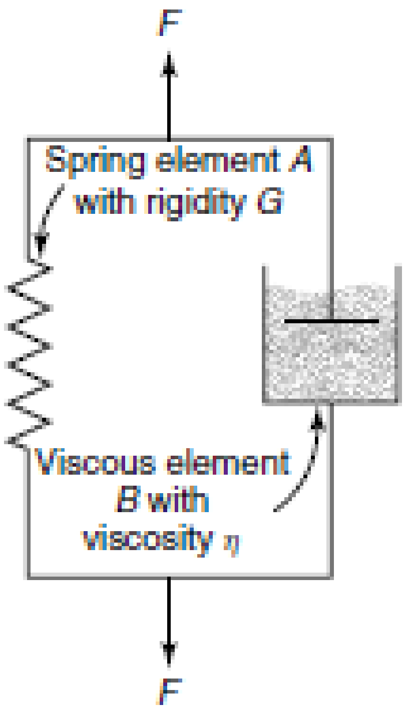

$$\tau = G\gamma + \eta \frac{d\gamma}{dt}$$

For constant stress $d\tau/dt = 0$

$$\gamma = \frac{\tau}{G}\left[1 - \exp\left(\frac{-Gt}{\eta}\right)\right]$$

$$\gamma_r = \frac{\tau}{G}\left[1 - \exp\left(\frac{-t}{t_{ret}}\right)\right]$$

$$t_{ret} = \eta / G$$

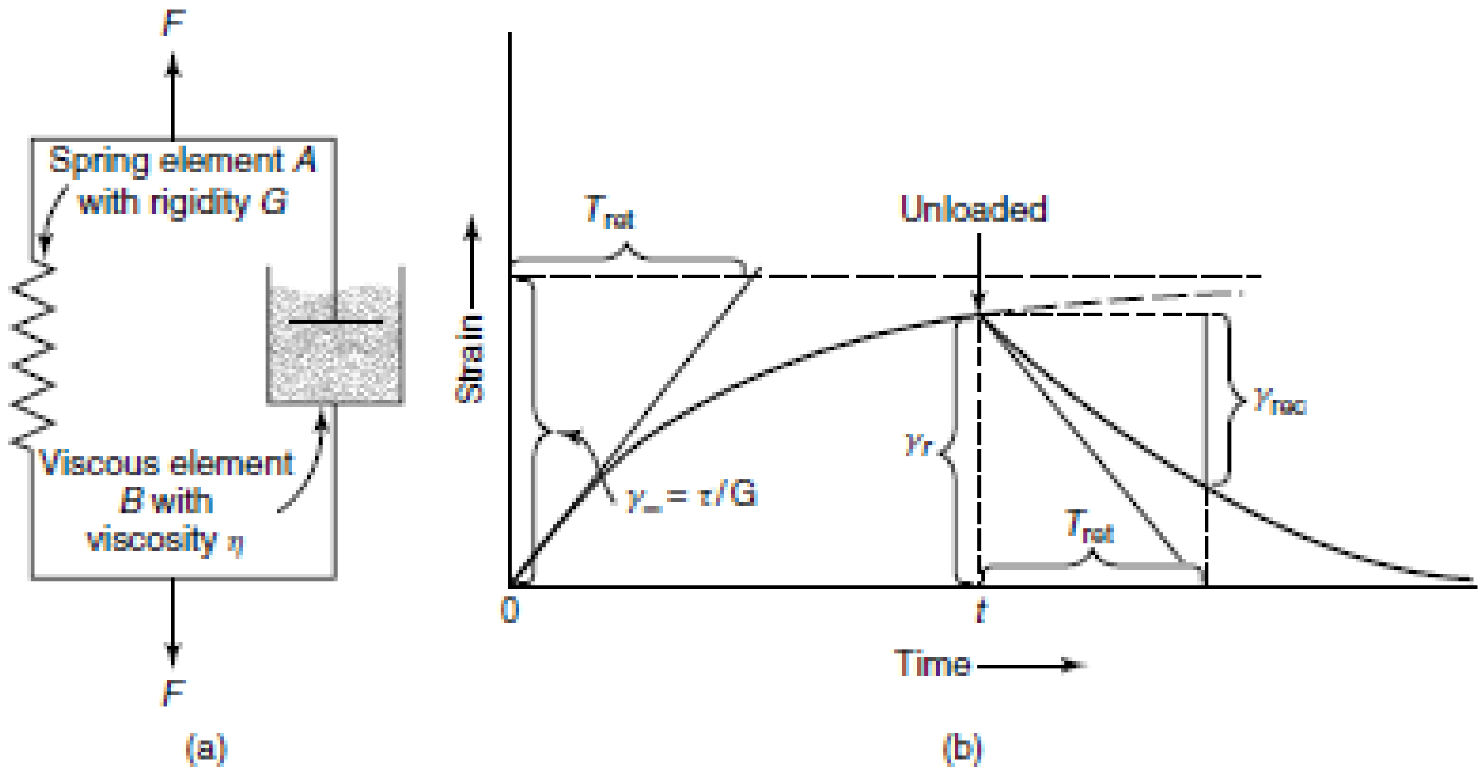

Figure 5.61 (a) Kelvin–Voigt spring and dashpot in parallel model of viscoelasticity and (b) resulting time-dependent strain. From Z. Jastrzebski, *The Nature and Properties of Engineering Materials*, 2nd ed. Copyright © 1976 by John Wiley & Sons, Inc. This material is used by permission of John Wiley & Sons, Inc.

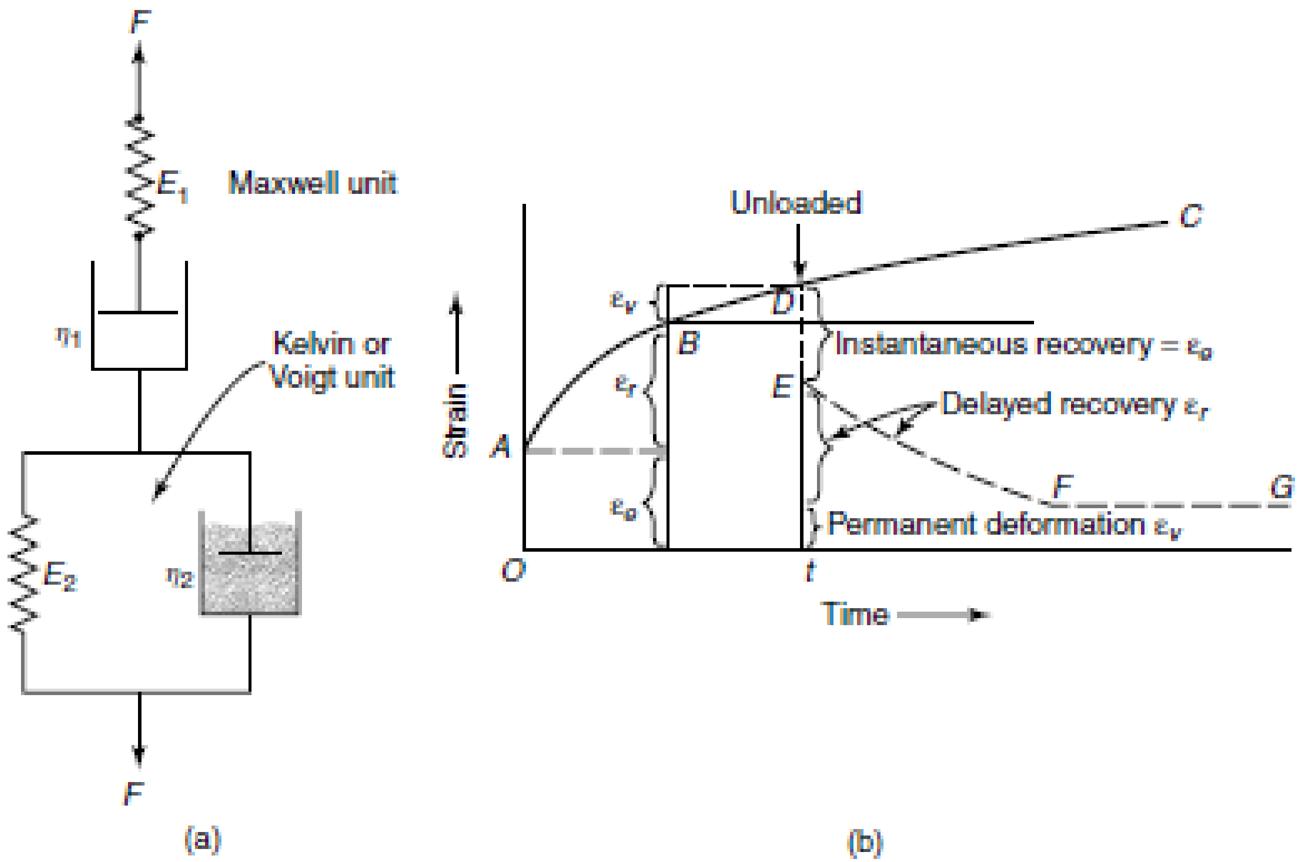

Figure 5.62 (a) Four-element spring and dashpot model of viscoelasticity and (b) resulting strain-dependent time diagram. From Z. Jastrzebski, *The Nature and Properties of Engineering Materials*, 2nd ed. Copyright © 1976 by John Wiley & Sons, Inc. This material is used by permission of John Wiley & Sons, Inc.

http://www.personal.psu.edu/irh1/SWF/SpringDashpot.swf

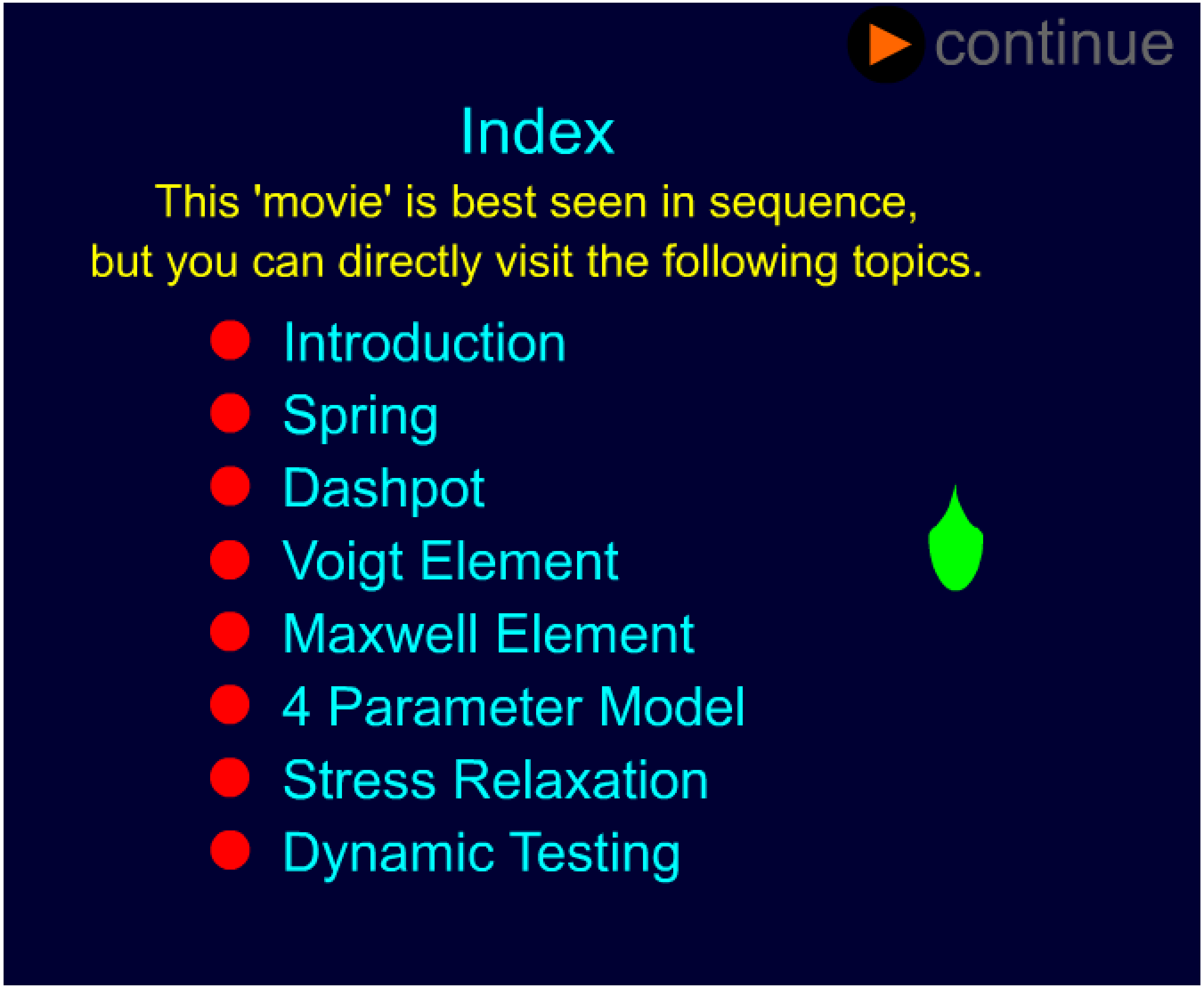

Maxwell Element

A spring and a dashpot in series show both instantaneous elastic character and viscous flow. This system also has a retardation time as defined for the Voigt element. The Maxwell element will be more useful modelling Stress Relaxation experiments.

$$\tau = \eta/E$$

continue

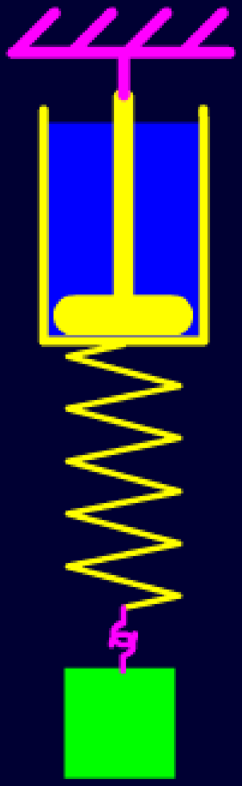

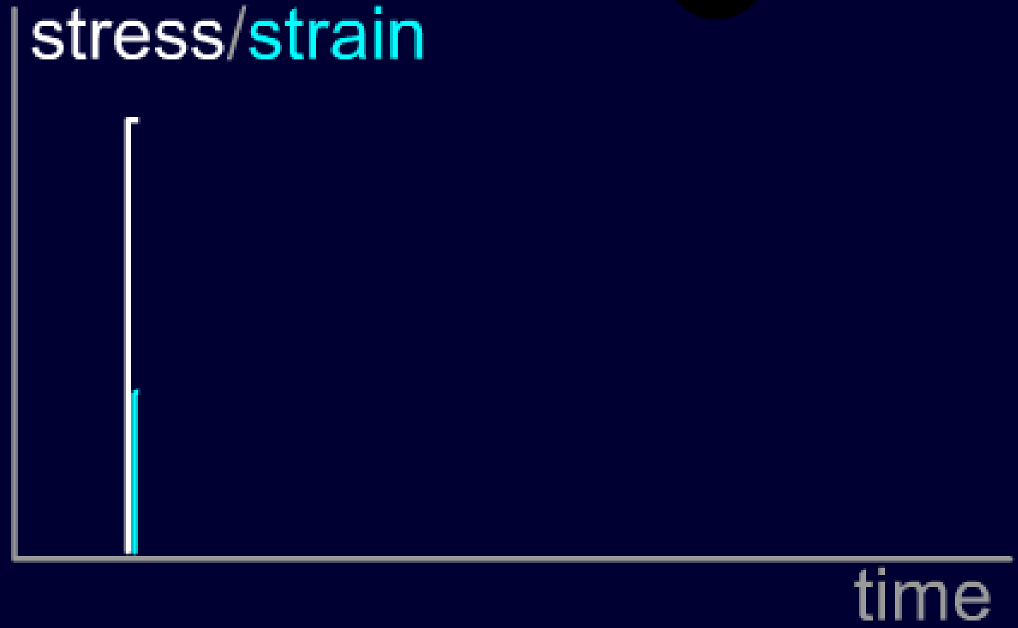

As soon as the system is loaded the spring can instantly deform.

Dashpots can't instantaneously respond to loading and initially the dashpot is undeformed.

continue

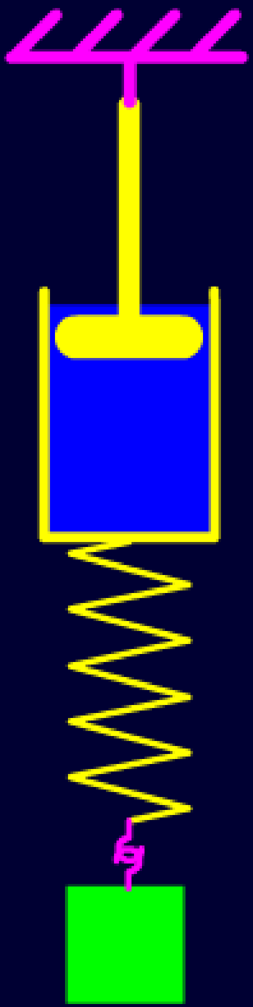

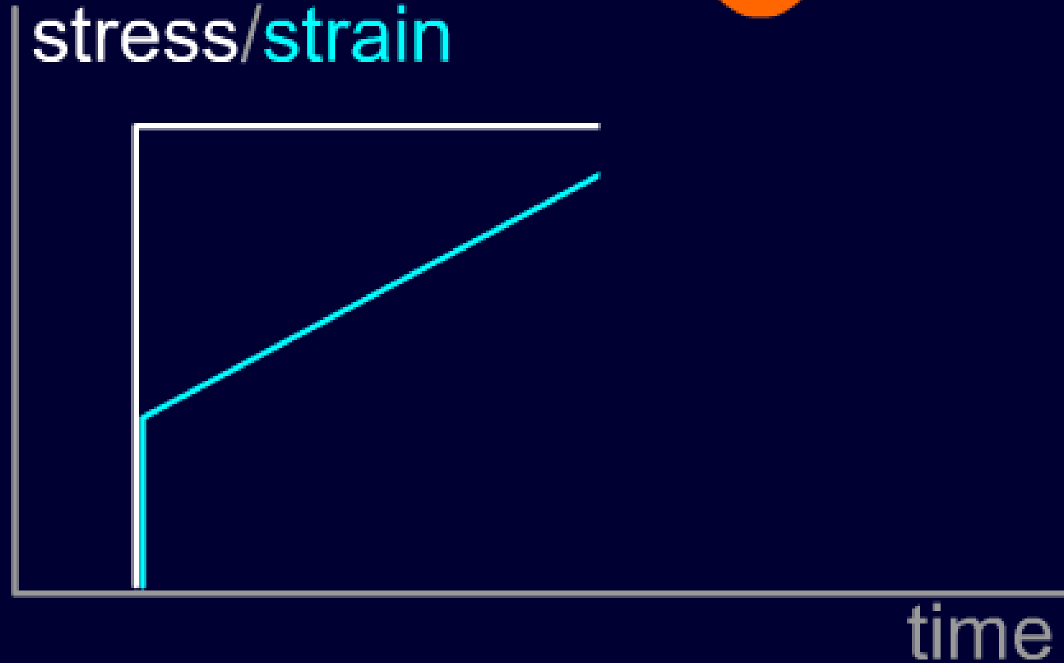

Since the load is also borne by the dashpot it will open up at an appropriate rate, proportional to load; and continue to do so as long as the load is applied.

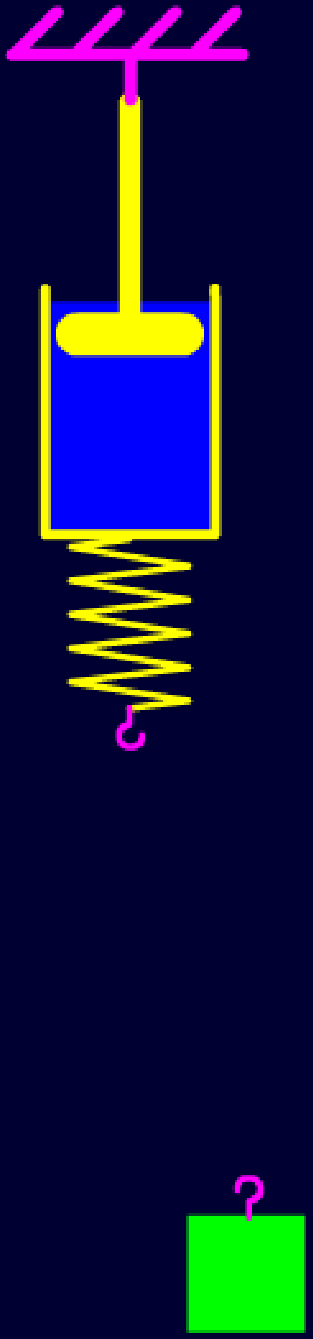

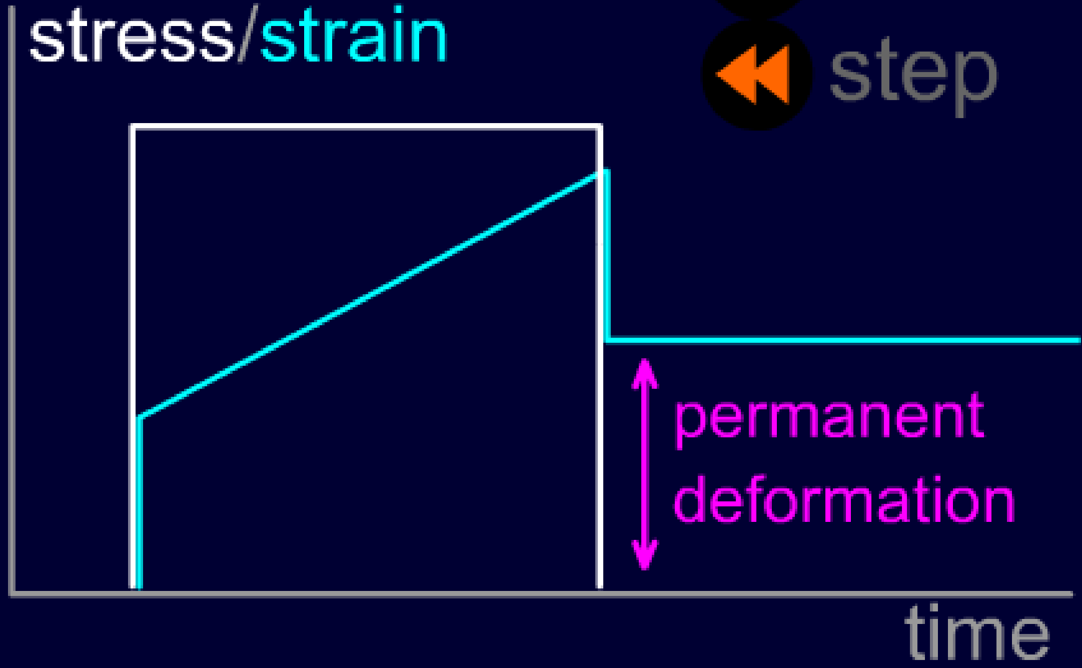

continue

step

When the load's removed the spring is able to instantly retract; the dashpot remains open (no restoring force). The net result is a system that shows permanent deformation from the dashpot opening up.

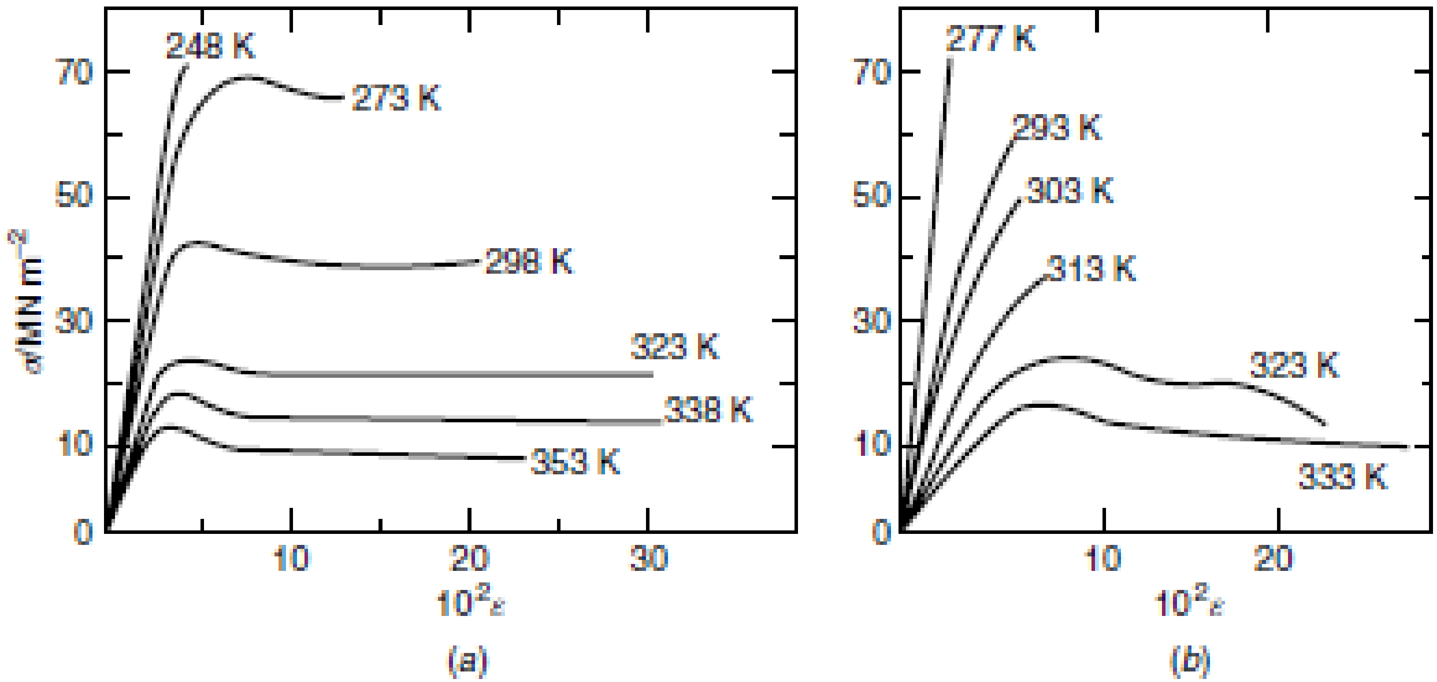

Figure 5.67 Influence of temperature on the stress–strain response of (a) cellulose acetate and (b) poly(methyl methacrylate). Reprinted, by permission, from J. M. G. Cowie, *Polymers: Chemistry & Physics of Modern Materials*, 2nd ed., p. 283. Copyright © 1991 by J. M. G. Cowie.

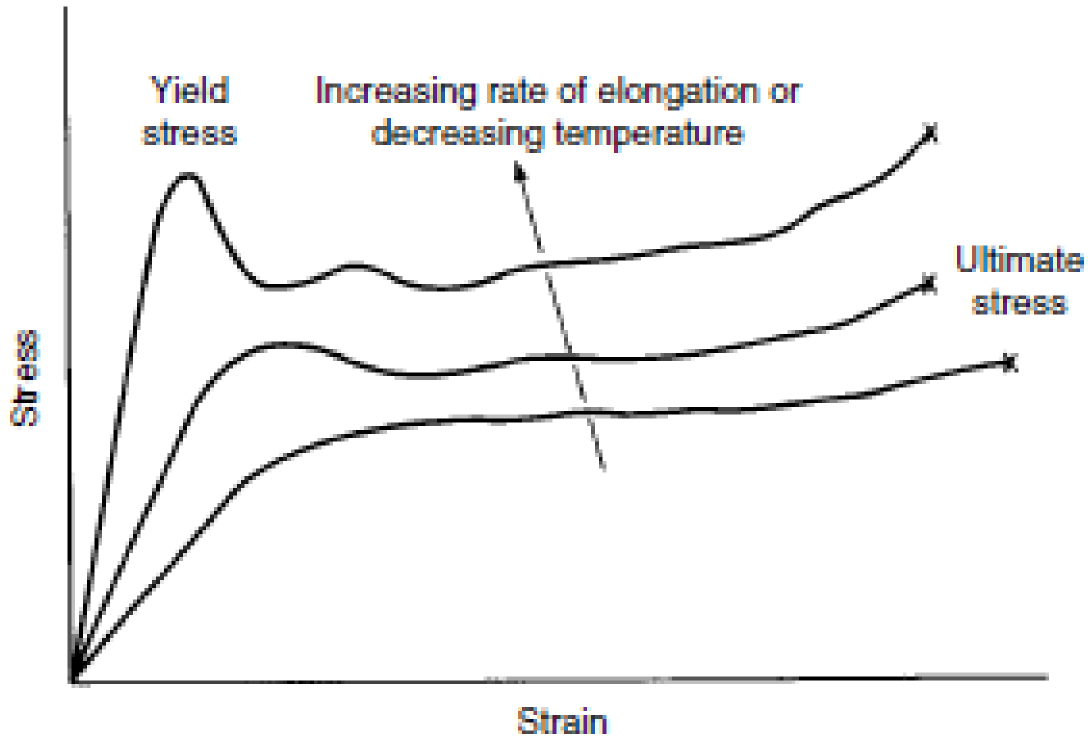

Figure 5.68 Effect of increasing strain rate and decreasing temperature on stress–strain curves for polyethylene. Reprinted, by permission, from F. Rodriguez, *Principles of Polymer Systems*, p. 249, 2nd ed. Copyright © 1982 by Hemisphere Publishing Corporation.

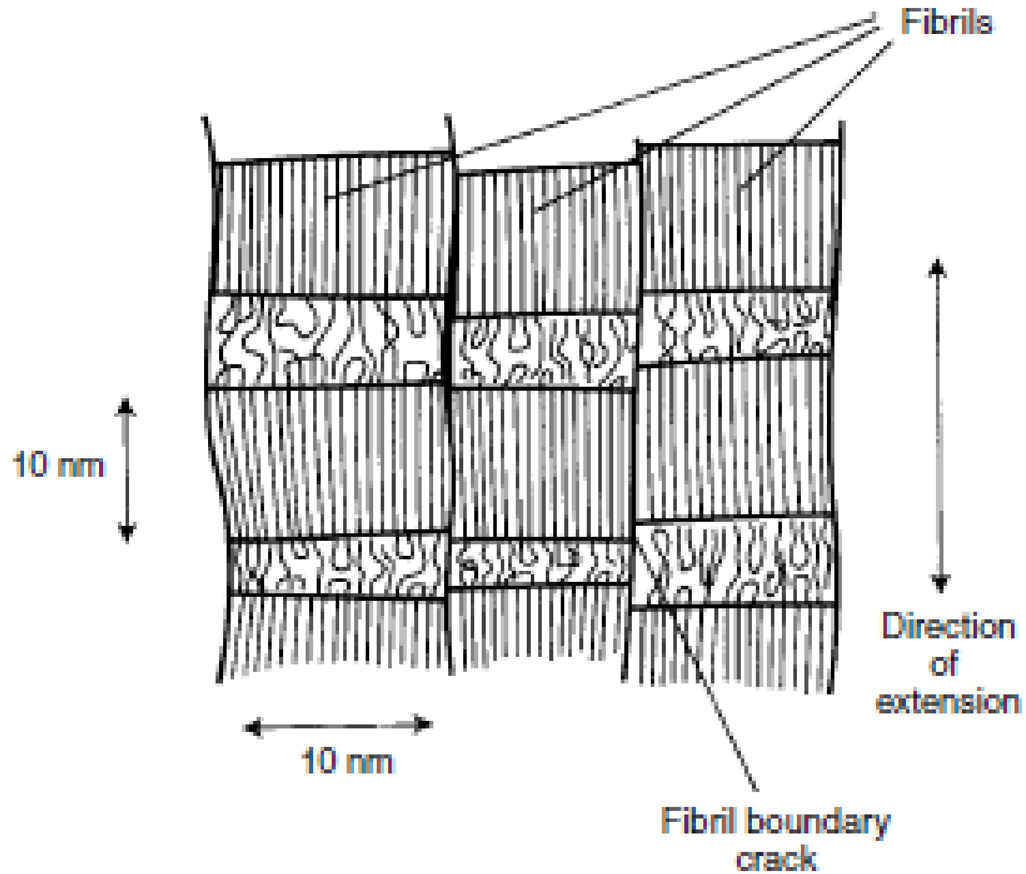

Figure 5.69 Fibrillar structure of an oriented polymer crystal as the result of an applied tensile force. Reprinted, by permission, from N. G. McCrum, C. P. Buckley, and C. B. Bucknall, *Principles of Polymer Engineering*, 2nd ed., p. 72. Copyright © 1997 by Oxford University Press.

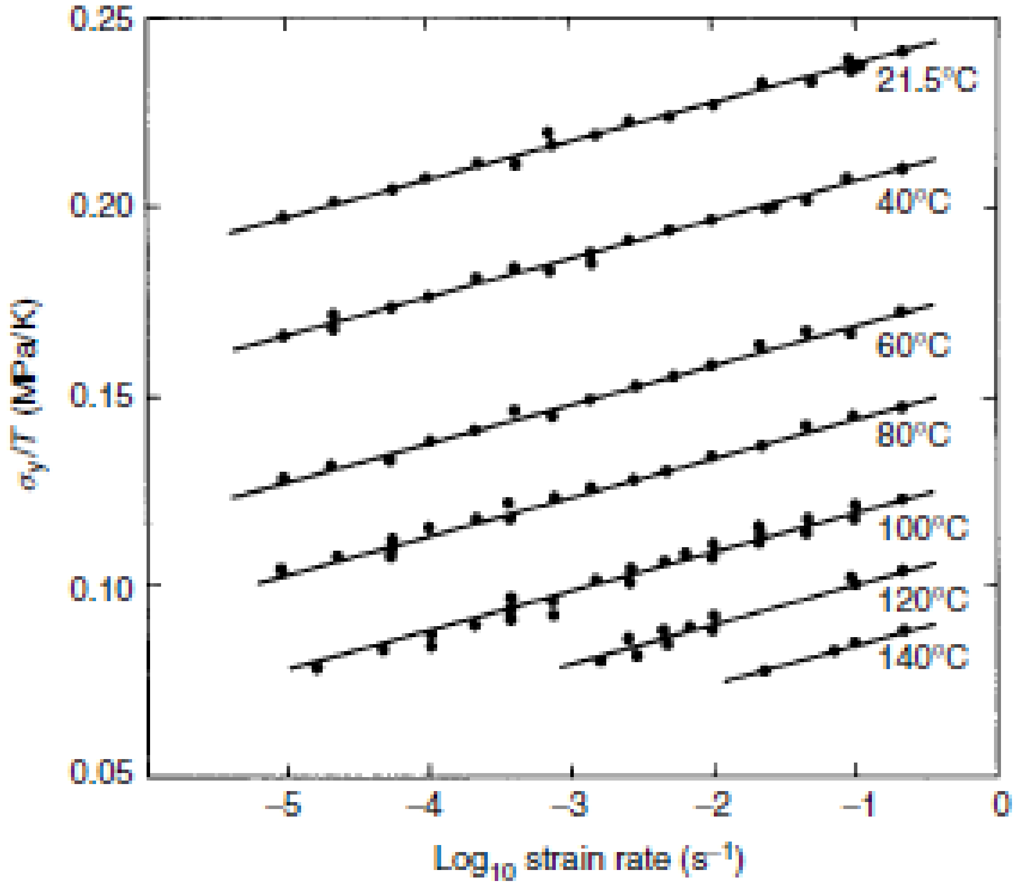

Figure 5.70 Eyring plot for polycarbonate. Reprinted, by permission, from N. G. McCrum, C. P. Buckley, and C. B. Bucknall, *Principles of Polymer Engineering*, 2nd ed., p. 191. Copyright © 1997 by Oxford University Press.

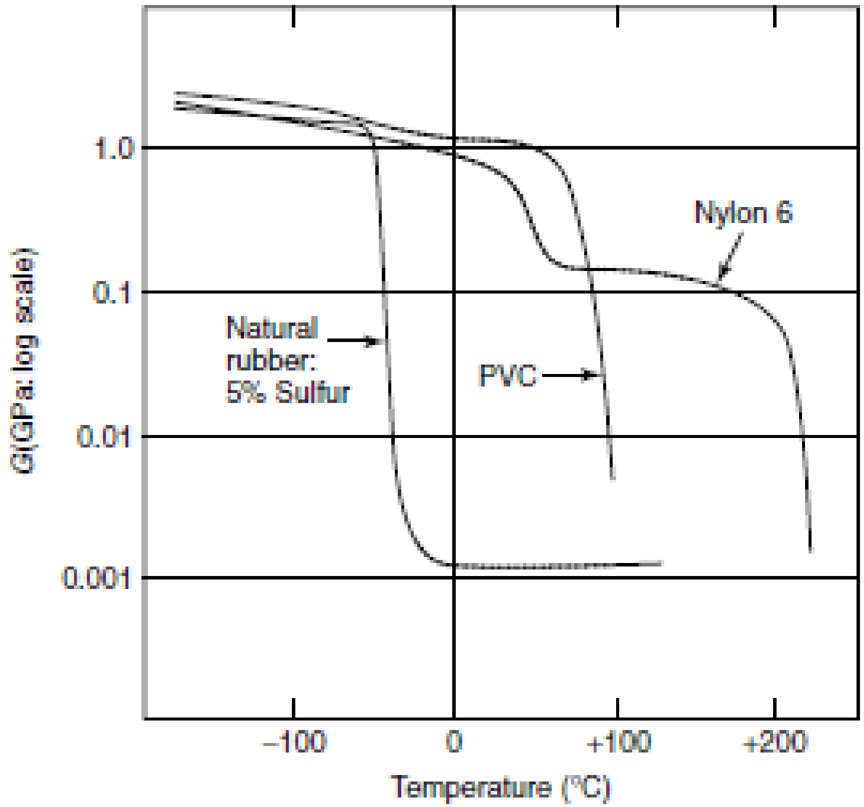

Figure 5.71 Dependence of shear modulus on temperature for three common engineering polymers: crosslinked natural rubber, amorphous polyvinyl chloride (PVC), and crystalline Nylon 6. The typical use temperatures are indicated by dotted lines. Reprinted, by permission, from N. G. McCrum, C. P. Buckley, and C. B. Bucknall, *Principles of Polymer Engineering*, 2nd ed., p. 154. Copyright © 1997 by Oxford University Press.

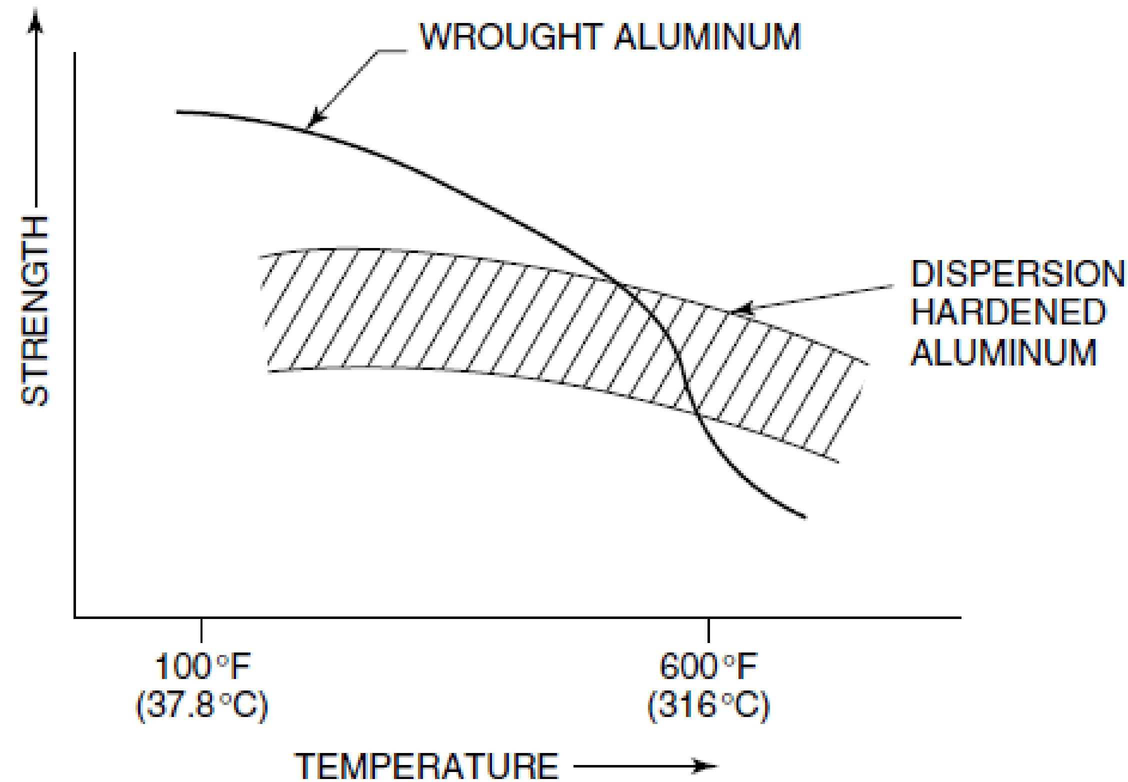

Figure 5.81 Strength of dispersion-strengthened aluminum compared with wrought aluminum. Reprinted, by permission, from M. Schwartz, *Composite Materials Handbook*, 2nd ed., p. 1.29. Copyright © 1992 McGraw-Hill Book Co.

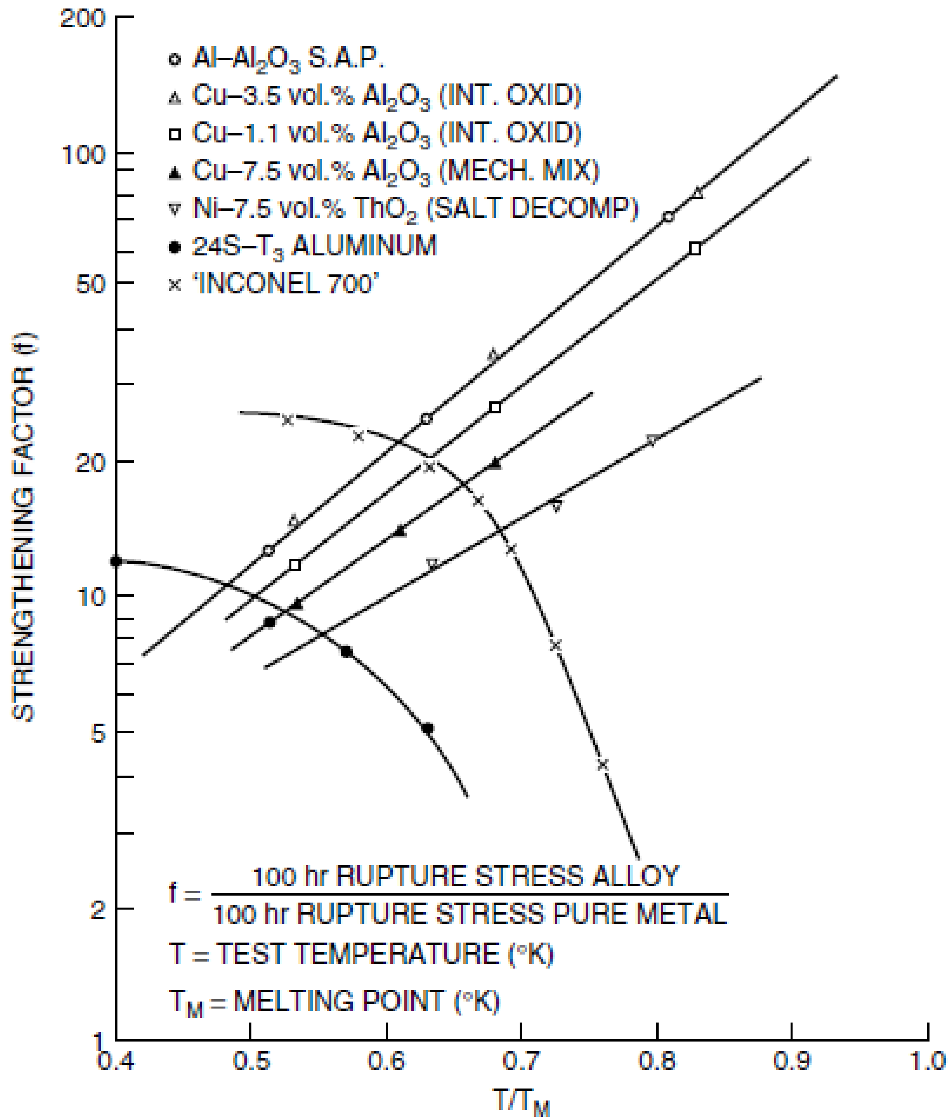

Figure 5.82 The strength of different dispersion-strengthened alloys relative to the pure metal strength as a function of relative temperature. Preparation techniques include sintered aluminum powder (SAP), internal oxidation, and salt decomposition. Reprinted, by permission, from A. Kelly, *Composite Materials*, p. 62. Copyright © 1966 by American Elsevier, Inc.

$$E_1 = V_f E_f + (1 - V_f) E_m$$

$$E_2 = \frac{E_f E_m}{(1 - V_f) E_f + V_f E_m}$$

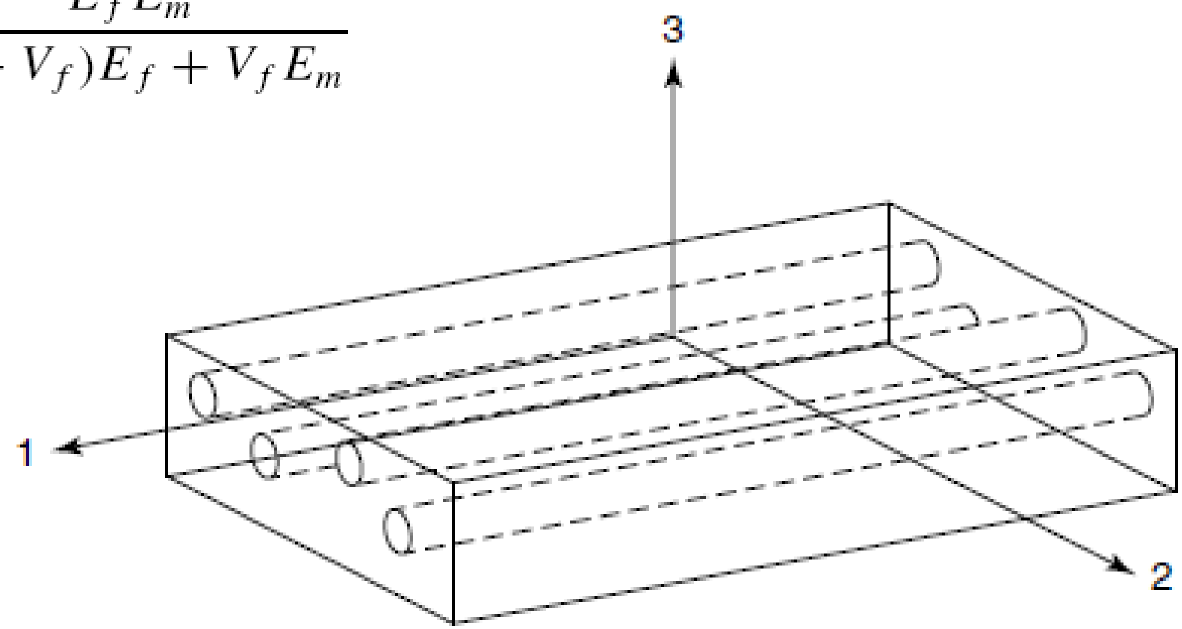

Figure 5.85 Definition of axes in a continuous, unidirectional fiber-reinforced composite. Reprinted, by permission, from N. G. McCrum, C. P. Buckley, and C. B. Bucknall, *Principles of Polymer Engineering*, 2nd ed., p. 258. Copyright © 1997 by Oxford University Press.

CASE STUDY

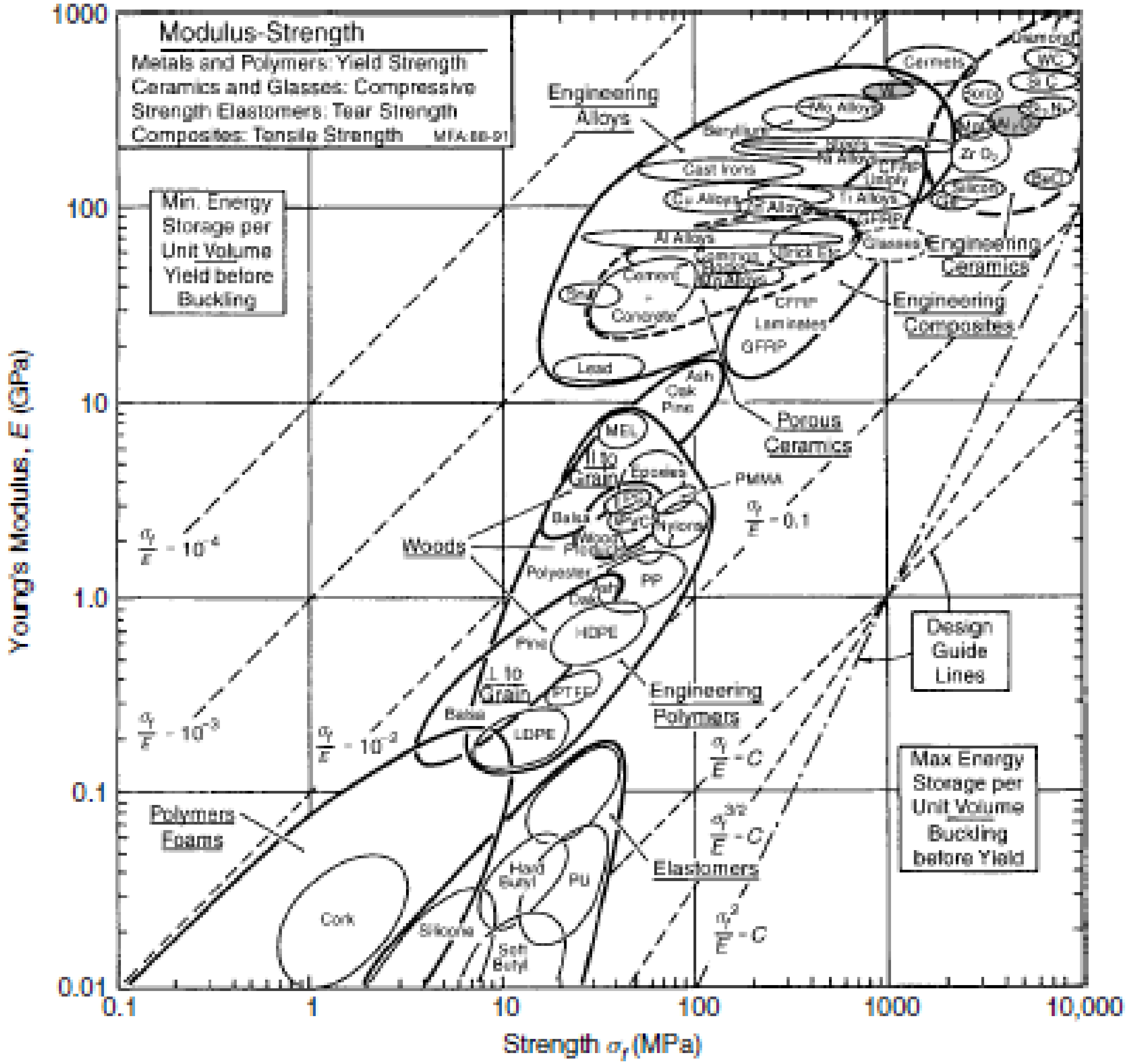

Figure 5.56 Design chart of modulus versus strength (see inset for type of strength determination). Reprinted, by permission, from M. F. Ashby, *Materials Selection in Mechanical Design*, 2nd ed., p. 42. Copyright © 1999 by Michael F. Ashby.

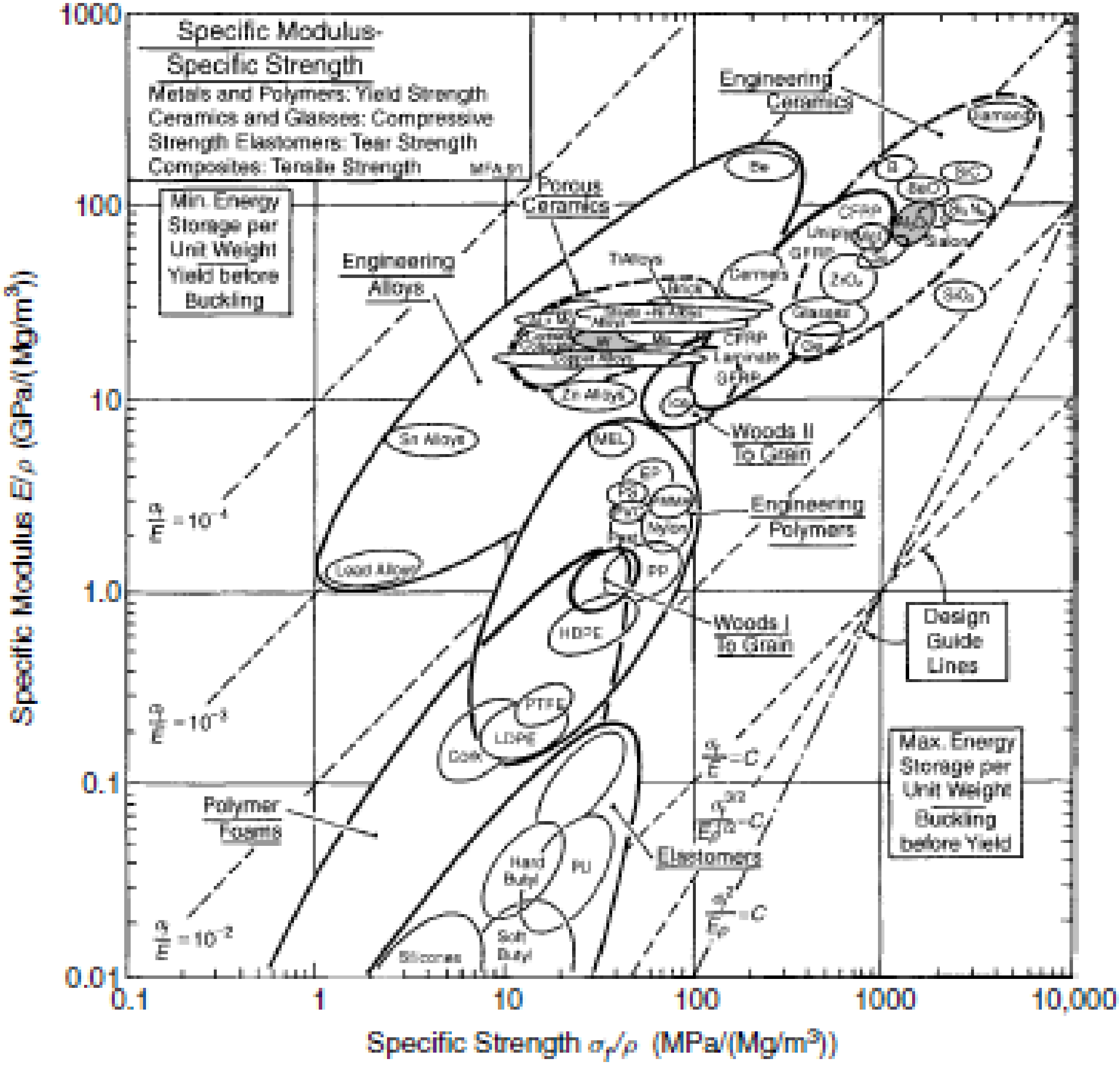

Figure 5.57 Design chart of specific modulus versus specific strength (see inset for type of strength determination). Reprinted, by permission, from M. F. Ashby, *Materials Selection in Mechanical Design*, 2nd ed., p. 44. Copyright © 1999 by Michael F. Ashby.